
Curvature Tuning: Provable Training-free Model Steering From a Single Parameter

Leyang Hu¹ Randall Balestriero¹

Abstract

The scaling of model size and data size has reshaped the paradigm of AI. As a result, the common protocol to leverage the latest models is to steer them towards a specific downstream task of interest through *fine-tuning*. Despite its importance, the main methods for fine-tuning remain limited to full or low-rank adapters—containing countless hyper-parameters and lacking interpretability. In this paper, we take a step back and demonstrate how novel and explainable post-training steering solutions can be derived theoretically from *spline operators*, a rich mathematical framing of Deep Networks that was recently developed. Our method—coined **Curvature Tuning (CT)**—has a single parameter that provably modulates the curvature of the model’s decision boundary henceforth allowing training-free steering. This makes CT both more efficient and interpretable than conventional fine-tuning methods. We empirically validate its effectiveness in improving generalization and robustness of pre-trained models. For example, CT improves out-of-distribution transfer performances of ResNet-18/50 by 2.57%/1.74% across seventeen downstream datasets, and improves RobustBench robust accuracy by 11.76%/348.44%. Additionally, we apply CT to ReLU-based Swin-T/S, improving their generalization on nine downstream datasets by 2.43%/3.33%. Our code is available at <https://github.com/Leon-Leyang/curvature-tuning>.

1. Introduction

The scaling of model and data sizes has given rise to foundation models, such as Llama3 (Dubey et al., 2024) for natural

¹Department of Computer Science, Brown University, Providence, RI, USA. Correspondence to: Leyang Hu <leyang.hu@brown.edu>, Randall Balestriero <randall.balestriero@brown.edu>.

language processing (NLP), DINOv2 (Oquab et al., 2023) for computer vision (CV), CLIP (Radford et al., 2021) and SigLIP (Zhai et al., 2023) for multimodal tasks, and OpenVLA (Kim et al., 2024) for embodied agent. These models are more universally capable than ever, accelerating a paradigm shift in artificial intelligence (AI): transitioning from training task-specific models from scratch to leveraging models pretrained on large datasets and fine-tuning them for downstream applications.

Full fine-tuning, the process of steering a pretrained model by adapting all its parameters to downstream datasets, was once the primary approach for transferring knowledge. While it effectively enhances generalization (Radford, 2018) and robustness (Jeddi et al., 2020), it is computationally expensive. To mitigate this, parameter-efficient fine-tuning (PEFT) methods such as Serial Adapter (Houlsby et al., 2019) and LoRA (Hu et al., 2021) have been introduced, which partially alleviate the computational burden (as further training is still required) by fine-tuning only a small subset of parameters. However, these approaches face two additional challenges: a lack of principled design and limited interpretability. For instance, they rely on heuristic choices—such as LoRA’s rank, placement, and initialization—with minimal theoretical guidance. Moreover, they treat the model as a black box, making it unclear how pretrained knowledge is preserved or how the model is steered for downstream tasks. This combination of partial efficiency, heuristic-driven design, and poor interpretability underscores the need for fine-tuning methods that are efficient, principled, and interpretable. We thus ask the following question: *How can we construct principled steering solutions addressing both efficiency and interpretability?*

We take a first step toward an overarching answer to how new PEFT solutions can be derived from theoretically grounded frameworks. Leveraging the spline framework of Deep Learning (Montufar et al., 2014; Balestriero et al., 2018), we develop a novel solution—**Curvature Tuning (CT)**—which modulates a model’s decision boundary curvature through a single parameter, β . CT offers several advantages, which we briefly outline below.

CT steers a model in inference mode without backpropagation. Since CT uses a single parameter to modulate the

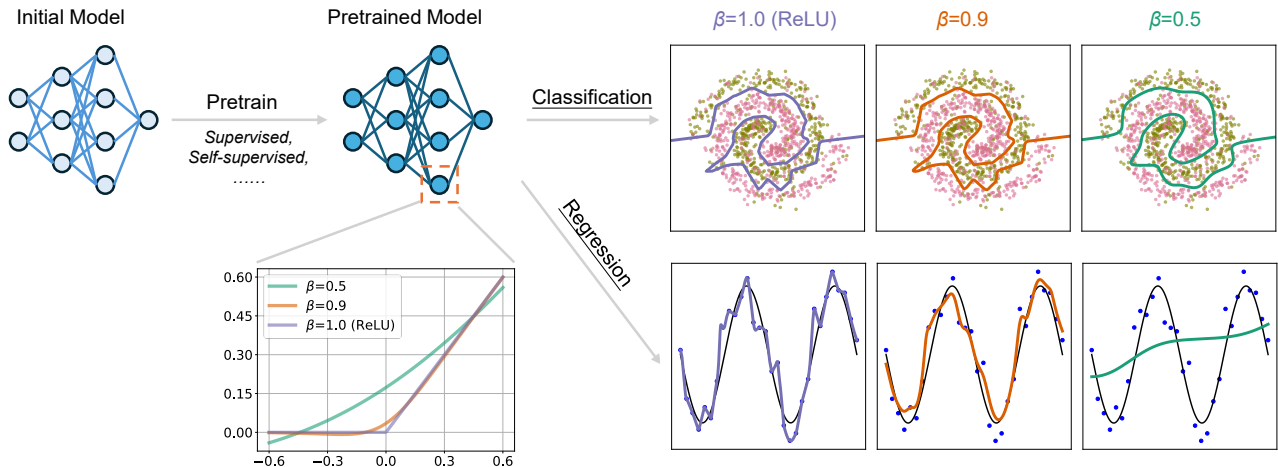


Figure 1: Illustration of the **Curvature Tuning (CT)** mechanism for model steering. **CT steers a pretrained model by replacing ReLUs with a β -parameterized activation function and tuning β from 1 to 0, progressively smoothing the model’s decision boundary across tasks (e.g., classification and regression).** The β -parameterized activation function is defined in Equation (7).

model’s curvature, its optimal value can be determined via cross-validation without requiring training or backpropagation. This property ensures maximal computational and memory efficiency.

CT is interpretable for any value of β . CT replaces internal activation functions such as ReLU and Leaky ReLU with a convex combination of a reparameterized Swish function (Ramachandran et al., 2017) and a Softplus function, controlled by the parameter β . This theoretically grounded construction directly modulates the model’s decision boundary curvature. When $\beta = 1$, the original activation function is recovered, resulting in a piecewise affine decision boundary. When $\beta = 0$, the model becomes entirely linear, making the decision boundary globally affine. Intermediate values of β gradually smooth the decision boundary, offering a continuous transition between these two extremes.

CT significantly improves a model’s performance across tasks and domains while enhancing robustness. We empirically validate the effectiveness of CT through extensive experiments, demonstrating improvements in both generalization and robustness. For same-task generalization, transferring ResNet-18 (He et al., 2016) across seventeen image classification datasets—including MNIST, CIFAR-10, CIFAR-100 (Krizhevsky et al., 2009), and ImageNet (Deng et al., 2009)—yields a relative accuracy gain of 2.57%. For cross-task generalization, CT achieves a relative improvement of 0.41% in the mIoU of a PSPNet (Zhao et al., 2017) using an ImageNet-pretrained ResNet-50 as backbone on VOC2012 (Everingham et al.). Moreover, CT delivers a relative improvement of 11.76% in the robust accuracy of an ImageNet-pretrained ResNet-18 on RobustBench (Croce et al., 2020). Additional experiments with models such as

ResNet-50/152, Swin-T/S, as well as additional datasets, further confirm CT’s effectiveness.

A visual depiction of the CT mechanism is shown in Figure 1, and our key contributions are summarized below:

- Theoretical Contribution:** We introduce Curvature Tuning (CT), a training-free model steering technique that provably adjusts the curvature of model decision boundaries using a single parameter. This principled design ensures both efficiency and interpretability. Details are provided in Section 3.
- Empirical Contribution:** We demonstrate in Section 4 that CT enhances generalization and robustness across various models, datasets, and tasks. For example, CT improves out-of-distribution transfer performances of ResNet-18/50 by 2.57%/1.74% across seventeen downstream datasets, and improves RobustBench robust accuracy by 11.76%/348.44%. It also improves generalization of ReLU-based Swin-T/S on nine downstream datasets by 2.43%/3.33%.

The remainder of this paper is organized as follows: Section 2 reviews current fine-tuning techniques and introduces relevant spline concepts, the foundation for our method. Section 3 details our proposed method and its theoretical guarantees. Section 4 presents experimental results, and Section 5 summarizes our findings and potential future directions.

2. Background

This section presents a concise review of current fine-tuning techniques and their limitations in Section 2.1, followed by an introduction to relevant concepts in splines and their connections to Deep Networks (DNs), which are foundational for understanding CT.

2.1. The Fine-tuning Menagery

Fine-tuning, in the context of this paper, refers to adapting a pretrained model to improve its ability to solve a particular downstream task of interest. Initially, the common practice was to take the downstream task and continue training all of the model parameters, a process commonly referred to as *full fine-tuning*. Notable examples include GPT (Radford, 2018) and DINO (Caron et al., 2021). However, as model sizes continue to grow, performing full fine-tuning on the latest models would require immense infrastructure and often result in poor performance due to the small size of many downstream task datasets. Given these challenges, *parameter-efficient fine-tuning (PEFT)* methods were developed to mitigate the cost while maintaining effectiveness.

To better understand the landscape of PEFT approaches, we adopt the categorization proposed by Han et al. (2024), which organizes these methods into four primary categories. **Additive PEFT** introduces additional trainable parameters to the pretrained model, training only these new parameters during fine-tuning. Examples include Serial Adapter (Houlsby et al., 2019), Prefix-tuning (Li & Liang, 2021), and (IA)³ (Liu et al., 2022). **Selective PEFT** identifies a subset of existing parameters for fine-tuning, with examples such as U-Diff pruning and S-Diff pruning (Guo et al., 2020). **Reparameterized PEFT**: decomposes pretrained weights into low-rank matrices, fine-tuning only the low-rank components, which are converted back during inference; examples include LoRA (Hu et al., 2021) and DyLoRA (Valipour et al., 2022). **Hybrid PEFT** combines multiple PEFT approaches, such as UniPELT (Mao et al., 2021) and S4 (Chen et al., 2023).

While these techniques vary in the parameters they modify, they all require further training, which remains computationally expensive. In particular, backpropagation presents significant challenges for larger models. Additionally, their application often involves tuning numerous hyperparameters, typically guided by heuristics with limited theoretical justification, making it difficult to determine optimal values. Moreover, deep learning training remains largely opaque, complicating the understanding of how pretrained knowledge is preserved and limiting interpretability. For instance, deploying LoRA involves multiple design choices, including selecting the layers where it should be applied (Gao et al., 2024), determining its rank (Valipour et al., 2022; Chen et al., 2024), choosing the scaling factor during inference

(Kalajdziewski, 2023), and initializing its parameters (Hayou et al., 2024), all of which rely primarily on heuristics. Furthermore, even with a low-rank configuration, fine-tuning LoRA variants of ResNets—relatively small models compared to contemporary large models—still requires tens of thousands to over a million parameters, as shown in Table 7.

In contrast, our proposed method, CT, bypasses training entirely, eliminating the need for backpropagation, significantly improving efficiency. Moreover, CT offers greater interpretability, as it directly and provably adjusts the model’s decision boundary, as demonstrated in later sections.

2.2. The Spline formulation of Deep Networks

In this subsection, we review relevant concepts in splines, which provide a mathematical framework for understanding the relationship between piecewise-affine functions and DNs.

A *spline function* is a function $s : \mathbb{R}^D \rightarrow \mathbb{R}$ defined piecewise by polynomials. An *affine spline function* is a special case where each piece is defined by an affine function. Such a function can be parameterized by three components:

- $\mathbf{A} \in \mathbb{R}^{R \times D}$: A matrix representing the slopes of the affine functions.
- $\mathbf{b} \in \mathbb{R}^R$: A vector representing the offsets of the affine functions.
- $\Omega \triangleq \{\omega_1, \dots, \omega_R\}$: A partition of the input space \mathbb{R}^D into R regions.

For an input $\mathbf{x} \in \mathbb{R}^D$, the affine spline function is defined as:

$$s[\mathbf{A}, \mathbf{b}, \omega](x) = \sum_{r=1}^R (\langle \mathbf{A}_{r,\cdot}, \mathbf{x} \rangle + \mathbf{b}_r) \mathbf{1}_{\{\mathbf{x} \in \omega_r\}}, \quad (1)$$

where $\mathbf{1}_{\{\mathbf{x} \in \omega_r\}}$ is an indicator function that equals 1 if \mathbf{x} belongs to region ω_r and 0 otherwise.

A *max-affine spline function* is a special case of an affine spline function that does not explicit knowledge of Ω . Instead, its output is computed as the maximum value over the affine functions:

$$s[\mathbf{A}, \mathbf{b}](\mathbf{x}) = \max_{r=1 \dots R} (\langle \mathbf{A}_{r,\cdot}, \mathbf{x} \rangle + \mathbf{b}_r) \quad (2)$$

The key result underpinning our study is that many deep network layers—such as fully connected layers, convolutional layers, and convex piecewise-affine activations (e.g., ReLU, max pooling, or maxout)—can be exactly represented as max-affine spline functions (Balestriero et al., 2018). Further details on this connection are provided in Appendix B.

While we primarily leverage this result from the spline formulation of deep networks, interested readers can refer to (Balestriero et al., 2019) for a deeper exploration of how the spline of each layer composes to make the entire input-output mapping of a DN an affine spline.

Now that we have reviewed the current fine-tuning methods and their limitations, and introduced relevant concepts in splines along with their connection to deep networks, which provide the theoretical foundation for our method, we proceed to present our proposed method in Section 3.

3. Curvature Tuning: A Provable Method for Model Steering

In this section, we introduce our proposed method, Curvature Tuning (CT). We first dive into its motivation and construction in Sections 3.1 and 3.2, followed by implementation details in Section 3.3. Readers focused on practical applications of CT will find our experiments in Section 4.

3.1. The β -VQ Inference Framework

To understand the motivation behind CT, we first conduct an in-depth study of the max-affine spline formulation from Equation (2).

By inspecting Equation (2), we observe that the mapping remains affine within each (implicitly defined) region where the pointwise maximum does not change. Specifically, for any input \mathbf{x} where

$$\arg \max_{r=1\dots R} (\langle \mathbf{A}_{r,\cdot}, \mathbf{x} \rangle + \mathbf{b}_r),$$

remains constant, all such inputs belong to the same region, as they share the same affine mapping. The nonlinearity of the function arises when transitioning between these regions.

For instance, in the case of ReLU, where $R = 2$, $\mathbf{A}_{2,\cdot} = \mathbf{0}$, and $\mathbf{b}_2 = 0$, the nonlinearity occurs along a hyperplane in the input space. Intuitively, a ReLU activation, which maps $\mathbb{R} \mapsto \mathbb{R}$, is nonlinear at 0. When preceded by an affine transformation (such as linear or convolutional layer) with input dimension D , this nonlinearity occurs along a hyperplane of dimension $D - 1$, defined by the layer’s parameters mapping the input space to that unit.

Smoothing the nonlinearity by smoothing the spline region assignment process. Instead of going from one affine mapping to another in an abrupt fashion (whenever crossing that hyperplane), one may consider a smoother transition. As far as we are aware, there are two common practices to achieve that goal. To get into details into each of them, we must first provide a slightly different formulation of the max-affine spline mapping.

We know that each unit of a layer is a max-affine spline. The inference process of each unit can thus be decomposed into two steps:

1. **VQ Inference Step (region selection):** Determine the affine transformation that maximizes the output, which can be viewed as a vector quantization process. The decision is encoded in a selection variable $\mathbf{t} \in \mathbb{R}^R$, where R is the number of input region partitions of the max-affine spline function. In a MASO setting, the selection variable \mathbf{t} is a one-hot vector with the r^* -th entry set to 1, where:

$$r^* = \arg \max_{r \in \{1, \dots, R\}} (\langle \mathbf{A}_{r,\cdot}, \mathbf{x} \rangle + \mathbf{b}_r). \quad (3)$$

2. **Computation Step (affine transformation):** Compute the output of the neuron based on the selection variable \mathbf{t} :

$$f(x) = \sum_{r=1}^R \mathbf{t}_r \cdot (\langle \mathbf{A}_{r,\cdot}, \mathbf{x} \rangle + \mathbf{b}_r). \quad (4)$$

As discussed, the affine transformation is selected in a "hard" manner where only the transformation that maximizes the output is chosen. Alternatively, a "soft" approach can be employed in which the selection variable \mathbf{t} is no longer a one-hot vector but is inferred in a probabilistic manner. To see that, we follow the probabilistic formulation from (Balestriero & Baraniuk, 2018) as introduce the following regularize region selection problem

$$\begin{aligned} \mathbf{t}_\beta &= \arg \max_{\mathbf{t} \in \Delta_R} \beta \sum_{r=1}^R \mathbf{t}_r \cdot (\langle \mathbf{A}_{r,\cdot}, \mathbf{x} \rangle + \mathbf{b}_r) + (1 - \beta)H(\mathbf{t}), \\ &= \frac{e^{\beta(\langle \mathbf{A}_{r^*,\cdot}, \mathbf{x} \rangle + \mathbf{b}_{r^*})/(1-\beta)}}{\sum_{i=1}^R e^{\beta(\langle \mathbf{A}_{i,\cdot}, \mathbf{x} \rangle + \mathbf{b}_i)/(1-\beta)}} \end{aligned} \quad (5)$$

where $H(\mathbf{t})$ represents the Shannon entropy of the selection variable, and Δ_R is the simplex in \mathbb{R}^R . With the Computation Step in Equation (4) and using a ReLU activation function, switching from $\beta = 1$ to $\beta = 0.5$ is provably equivalent to replacing the ReLU with a sigmoid Gated Linear Unit. And in the limit of employing $\beta = 0$, the activation function becomes linear—and so does the entire input-output mapping of the DN.

Smoothing the nonlinearity by smoothing the max. As previously mentioned, there is an alternative way to smooth the max-affine spline mapping from Equation (2). Instead of relying on a soft region assignment, we can instead directly smooth the maximum function. It is already well known that smoothing the maximum operator leads to the log-sum-exp operator. Hence, the mapping from Equation (2) now

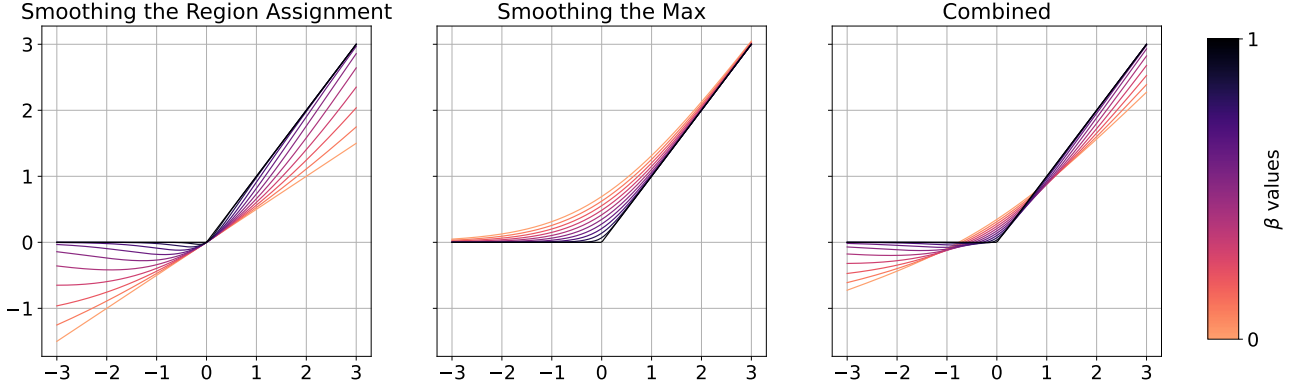


Figure 2: Visualization of nonlinearity smoothing through region assignment smoothing, max smoothing, and their combination. **The combined approach mitigates the opposing biases introduced by the individual methods.**

becomes

$$(1 - \beta) \log\left(\sum_{r=1}^R \exp((\mathbf{A}_r \cdot \mathbf{x}) + \mathbf{b}_r) / (1 - \beta)\right), \quad (6)$$

where we parametrized the mapping so that its behavior is akin to Equation (5), a value of $\beta \rightarrow 1$ recovers the original affine spline activation, e.g., ReLU.

The crucial observation that we make is that both parametrizations have a tendency to shift the mean of the output of the unit either by a negative factor (for Equation (5)) or by a positive factor (for Equation (6)). This means that in very deep models, varying β with either parametrization produces a shift in the decision boundary or regression that can not be recovered unless the parameters are trained once again—which we are trying to avoid. As a result, and as will be thoroughly detailed in Section 3.3, our implementation will leverage the average of the two parametrizations, mitigating that bias as depicted in Figure 2.

3.2. Provably Tuning Decision Curvature and Mitigating Drift

Prior to deriving our proposed CT methodology relying on the smoothness of activation functions derived in Section 3.1, we propose some characterization of a model’s curvature as a function of β .

We start by recalling the observations that for both parametrizations, we have that as $\beta \rightarrow 0$ as the activation becomes linear. Because all current DNs can be formulated as simple compositions of activation functions interleaved with affine operators, it is direct to see that the entire input-output mapping also becomes a simple affine mapping when $\beta \rightarrow 0$. In that setting, the curvature of the mapping—defined as the norm of the Hessian matrix of the mapping—will be 0. As a result, we see that as we go from the original DN map-

ping ($\beta = 1$) to the linear setting, we modulate the mapping curvature, and in particular we reduce it from its original value to 0 in the limit. When considering a classification task, the output of the DN is processed by a linear classifier. However, it is clear that as the DN’s mapping becomes more and more akin to a simple affine mapping, as the decision boundary also converges to being linear in the input space. This is exemplified in Figure 1.

3.3. Curvature Tuning (CT): Implementation

The implementation of CT is straightforward building upon Section 3.1 (PyTorch implementation in Appendix C). To apply CT, we replace all ReLU activation functions in the pretrained model with a custom activation function defined as:

$$f(x) = 0.5\sigma\left(\frac{\beta x}{1 - \beta}\right) \cdot x + 0.5 \log_e\left(1 + e^{\frac{x}{1 - \beta}}\right) \cdot (1 - \beta), \quad (7)$$

where $\sigma(\cdot)$ represents the sigmoid function.

This activation function is essentially a convex combination of a reparameterized Swish function and a reparameterized SoftPlus function, defined as:

$$\text{Swish}(x) = \sigma(\eta x) \cdot x, \quad \eta = \frac{\beta}{1 - \beta}, \quad (8)$$

$$\text{SoftPlus}(x) = \frac{1}{\gamma} \cdot \log(1 + e^{\gamma x}), \quad \gamma = \frac{1}{1 - \beta}. \quad (9)$$

Next, we determine the optimal value of β by performing forward passes on the test set, evaluating the model’s performance for each candidate β in a predefined range, and selecting the value that corresponds to the best-performing model. This process eliminates the need for additional training (i.e. backpropagation), making CT computationally efficient.

4. Curvature Tuning: Enhancing Model Generalization and Robustness

In this section, we empirically validate the effectiveness of CT by demonstrating its ability to improve model generalization on natural image classification (Section 4.1), as well as on medical image classification and more fine-grained tasks (Section 4.2). Additionally, we show that CT enhances robustness against adversarial and corrupted data (Section 4.3). We then demonstrate that CT is effective for transformers, even with partial theoretical guarantees (Section 4.4). Finally, we conduct ablation studies on its implementation in Section 4.5.

For all experiments, the parameter β is searched within the range $[0.5, 1)$ with a step size of 0.01. Each result is reported as the mean across three independent runs with seeds 42, 43, and 44. Additional experimental details and full results with standard deviations are provided in Appendix D.

4.1. Improving Generalization on Natural Image Datasets

In this subsection, we evaluate the effectiveness of CT in improving model generalization across natural image classification datasets through two experiments:

1. **Cross-Dataset Transfer:** We pretrain ResNet-18, ResNet-50, and ResNet-152 on MNIST, CIFAR-10, CIFAR-100, or ImageNet, apply CT to the pretrained model, and evaluate its performance when transferred to the remaining datasets¹. This experiment assesses CT’s impact when models are pretrained and transferred across datasets of varying sizes.
2. **ImageNet-to-Multiple-Datasets Transfer:** We apply CT to ImageNet-pretrained ResNet-18, ResNet-50, and ResNet-152 before transferring them to 9 additional datasets: Arabic Characters (El-Sawy et al., 2017), Arabic Digits (El-Sawy et al., 2016), Beans (Makerere AI Lab, 2020), CUB-200-2011 (Wah et al., 2011), DTD (Cimpoi et al., 2014), Fashion MNIST (Xiao et al., 2017), FGVC-Aircraft (Maji et al., 2013), Flowers102 (Nilsback & Zisserman, 2008), Food101 (Bossard et al., 2014). This experiment evaluates CT in a more realistic setting, where ImageNet-pretrained models are commonly used for downstream tasks.

While CT is applied consistently, the transfer learning approach differs depending on the dataset. For the same dataset (test set evaluation), the model is directly tested after applying CT, whereas for a new dataset transfer, the classification layer is removed, and linear probing (via logistic regression) is used for evaluation.

¹We exclude transfers to ImageNet due to computational costs.

Table 1 presents the results of the first experiment for ResNet-18. The complete results, including ResNet-50 and ResNet-152, are provided in Table 8. CT consistently improves generalization across models and datasets, yielding average relative accuracy gains of 1.68%, 1.96%, and 0.40% for ResNet-18, ResNet-50, and ResNet-152, respectively. Notably, in 25 out of 27 transfer cases, CT enhances accuracy. Even when evaluated on the test set of the pretraining dataset—where distribution shift is minimal—CT still provides improvements in 50% of cases, albeit with reduced effectiveness. Additionally, the average β values² for the three models are 0.82, 0.89, and 0.95—values close to 1. This suggests that CT efficiently identifies an appropriate β .

To validate CT’s robustness³ under different linear probing configurations, we provide additional experiments in Appendix D.2.

The results for the second experiment is shown in Table 2. CT improves performance in 26 out of 27 cases, achieving average relative improvements of 3.53%, 1.36%, and 0.77% for ResNet-18, ResNet-50, and ResNet-152, respectively. These improvements even exceed those in the first part of the experiment, further highlighting CT’s effectiveness in real-world generalization scenarios. Moreover, the average β values are 0.80, 0.93, and 0.95, respectively, once again demonstrating CT’s efficiency. Additionally, we provide visualizations of accuracy trends during the β search process in Figure 3, showing a sharp increase leading to a distinct peak, followed by a gradual decline as β increases.

In summary, our results demonstrate that CT effectively enhances model generalization across natural image classification datasets. In the following section, we extend this analysis to medical image datasets and more fine-grained tasks to further assess CT’s impact on generalization.

4.2. Improving Generalization on Medical Image Datasets and Fine-grained Tasks

In this subsection, we further evaluate CT’s impact on model generalization in more complex scenarios, specifically on medical image datasets and more fine-grained tasks than single-label classification:

1. **Medical Image Datasets:** We apply CT to ImageNet-pretrained ResNet-18, ResNet-50, and ResNet-152 before transferring them to three medical image datasets: PathMNIST, OCTMNIST, and DermaMNIST from MedMNIST (Yang et al., 2023).
2. **Fine-grained Tasks:** We apply CT to ImageNet-pretrained ResNet-18, ResNet-50, and ResNet-152 for more fine-grained downstream tasks beyond single-

²Computed only for cases where improvements are observed.

³Referring to the robustness of CT itself, not the models.

Table 1: Accuracy of ResNet-18 trained and tested across MNIST, CIFAR-10, CIFAR-100, and ImageNet (**bold** entries indicate improvement with CT). **CT consistently enhances generalization across models and datasets, with β values close to 1**. Reported values are means over three runs; the complete results for ResNet-18, ResNet-50, and ResNet-152, including standard deviations, are provided in Table 8.

Test	Train	MNIST			CIFAR-10			CIFAR-100			ImageNet		
		ReLU (%)	+ CT (%)	(β)	ReLU (%)	+ CT (%)	(β)	ReLU (%)	+ CT (%)	(β)	ReLU (%)	+ CT (%)	(β)
MNIST		99.59	99.59	1.00	86.08	87.30	0.92	89.56	92.85	0.88	98.10	98.95	0.68
CIFAR-10		45.02	47.68	0.51	94.87	94.87	1.00	76.03	76.90	0.92	85.68	85.83	0.93
CIFAR-100		20.30	21.80	0.51	35.21	35.61	0.97	76.19	76.21	0.97	63.15	63.15	1.00
ImageNet		-	-	-	-	-	-	-	-	-	69.76	69.84	0.94

Table 2: Accuracy of ImageNet-pretrained ResNet-18, ResNet-50, and ResNet-152 when transferred to 9 downstream datasets (**bold** entries indicate improvement with CT). **CT consistently enhances generalization across models and datasets, with β values close to 1**. Reported values are means over three runs; the complete results, including standard deviations, are provided in Table 9.

Dataset	Model	ResNet-18			ResNet-50			ResNet-152		
		ReLU (%)	+ CT (%)	(β)	ReLU (%)	+ CT (%)	(β)	ReLU (%)	+ CT (%)	(β)
Arabic Characters		86.46	92.11	0.70	88.02	89.87	0.91	87.86	88.70	0.95
Arabic Digits		97.92	98.92	0.72	98.70	98.79	0.87	98.23	98.55	0.95
Beans		85.94	94.53	0.60	93.75	94.79	0.94	91.41	93.75	0.91
CUB-200-2011		62.93	63.60	0.90	66.09	66.57	0.93	68.76	69.74	0.94
DTD		64.38	64.50	0.92	70.46	70.82	0.95	70.48	70.57	0.98
Fashion MNIST		88.54	89.52	0.87	90.99	91.30	0.94	90.48	90.84	0.93
FGVC-Aircraft		43.75	48.30	0.77	47.62	51.09	0.89	49.93	50.35	0.94
Flowers102		87.80	87.96	0.86	89.56	89.56	1.00	88.97	89.15	0.96
Food101		59.70	60.48	0.89	68.07	68.13	0.97	70.95	71.02	0.99
Avg Rel Improve & β		Rel Improve (%) (β)			Rel Improve (%) (β)			Rel Improve (%) (β)		
		3.53 0.80			1.36 0.93			0.77 0.95		

label classification, including multi-label prediction on CelebA (Liu et al., 2015), regression on dSprites (Matthey et al., 2017)⁴, and semantic segmentation on VOC2012 (Everingham et al.)⁵. Detailed settings are provided in Appendix D.3.

The results, summarized in Table 3, show that CT consistently enhances generalization across these more challenging datasets and tasks. CT achieves average relative improvements of 2.69%, 1.74%, and 4.25% for ResNet-18, ResNet-50, and ResNet-152, respectively. Additionally, the average β values—0.83, 0.86, and 0.85—further underscore CT’s effectiveness and efficiency in complex scenarios.

Furthermore, we compare per-attribute accuracy, balanced accuracy, and F1-score of an ImageNet-pretrained ResNet-18/50/152 when transferred to multi-label prediction on CelebA, evaluating two selection methods for β : one optimized per attribute based on the best metric value and one using a globally optimal β selected for the highest mean accuracy across attributes. Table 4 presents the partial results for ResNet-18, while complete results for all models are provided in Table 13, Table 14, Table 15, Table 16, Table 17 and Table 18. The performance gap between the two methods is minimal: using a globally optimal β results in an average relative reduction of 0.21%/0.18%/0.07% in accuracy, 0.96%/0.65%/0.30% in balanced accuracy, and

⁴We regress the orientation of the shapes in dSprites.

⁵Only tested on ResNet-50 due to the architecture of the PSP-Net used.

2.81%/1.87%/1.00% in F1-score for ResNet-18/50/152 compared to per-attribute optimization. These results highlight the stability of CT in fine-grained downstream tasks like multi-label prediction.

In conclusion, we demonstrate that CT significantly improves model generalization even in more challenging settings, including medical imaging and fine-grained tasks. Next, we investigate its role in enhancing model robustness.

4.3. Improving Robustness on Adversarial and Corrupted Data

In this subsection, we demonstrate that CT enhances model robustness using RobustBench (Croce et al., 2020), a standardized benchmark for evaluating model robustness. RobustBench includes both adversarial examples, such as ℓ_2 and ℓ_∞ -norm bounded perturbations, which measure a model’s resistance to adversarial changes, and naturally corrupted examples (Hendrycks & Dietterich, 2019), such as noise and fog, which assess model’s robustness to real-world data distribution shifts.

To assess CT’s impact, we apply it to ImageNet-pretrained ResNet-18, ResNet-50, and ResNet-152 and evaluate their robustness on CIFAR-10, CIFAR-100, and ImageNet under both adversarial attacks (ℓ_2 and ℓ_∞) and corruption-based distortions. For each dataset, we sample 1,000 instances for evaluation. More detailed settings are provided in Appendix D.4.

As summarized in Table 19, CT consistently improves

Table 3: Performance of ImageNet-pretrained ResNet-18, ResNet-50, and ResNet-152 when transferred to challenging medical image datasets and fine-grained tasks (**bold** entries indicate improvement with CT). **CT consistently improves generalization across diverse datasets and tasks.** Reported values are means over three runs; the complete results, including standard deviations, are provided in Table 12.

(a) **ResNet-18.** Avg rel improve: 2.69%. Avg β : 0.83.

Dataset	Metric	ReLU	+ CT	Rel Improve (%)	(β)
PathMNIST	Acc (%) \uparrow	86.21	87.27	1.23	0.81
OCTMNIST	Acc (%) \uparrow	65.47	69.00	5.40	0.80
DermaMNIST	Acc (%) \uparrow	73.44	77.74	5.86	0.80
CelebA	Mean Acc (%) \uparrow	87.88	88.44	0.64	0.75
dSprites	MSE \downarrow	4.09	4.08	0.33	0.98
VOC2012	mIoU \uparrow	-	-	-	-

(b) **ResNet-50.** Avg rel improve: 1.74%. Avg β : 0.86.

Dataset	Metric	ReLU	+ CT	Rel Improve (%)	(β)
PathMNIST	Acc (%) \uparrow	89.83	89.88	0.06	0.98
OCTMNIST	Acc (%) \uparrow	68.60	69.93	1.94	0.90
DermaMNIST	Acc (%) \uparrow	73.67	77.44	5.12	0.89
CelebA	Mean Acc (%) \uparrow	89.18	89.42	0.27	0.91
dSprites	MSE \downarrow	4.40	4.28	2.62	0.53
VOC2012	mIoU \uparrow	0.68	0.69	0.41	0.96

(c) **ResNet-152.** Avg rel improve: 4.25%. Avg β : 0.85.

Dataset	Metric	ReLU	+ CT	Rel Improve (%)	(β)
PathMNIST	Acc (%) \uparrow	90.15	90.75	0.66	0.92
OCTMNIST	Acc (%) \uparrow	70.23	71.03	1.14	0.98
DermaMNIST	Acc (%) \uparrow	74.39	77.92	4.75	0.93
CelebA	Mean Acc (%) \uparrow	89.16	89.40	0.27	0.92
dSprites	MSE \downarrow	4.46	3.82	14.27	0.52
VOC2012	mIoU \uparrow	-	-	-	-

model robustness across the tested scenarios, achieving average relative improvements in robust accuracy⁶ of 11.76%, 348.44%, and 498.41% for ResNet-18, ResNet-50, and ResNet-152, respectively. Notably, the trend of increasing improvements as model size grows suggests that CT has the potential to be even more effective for larger models.

Moreover, the average β values are even closer to 1 compared to the generalization experiments, with values of 0.92, 0.95, and 0.98 for the three models, highlighting CT’s efficiency in optimizing robustness.

These results demonstrate that CT effectively enhances the robustness of pretrained models against both adversarial perturbations and common corruptions, further reinforcing its practical benefits. Having demonstrated CT’s impact on generalization and robustness in models that fully comply with the max-affine spline framework, where curvature tuning is provable from an end-to-end perspective, we now show that CT also works for transformers, where curvature tuning is only provable from a layer-wise perspective.

⁶Cases where the ReLU baseline has zero robust accuracy are excluded from computation.

Table 4: Comparison of per-attribute accuracy, balanced accuracy, and F1-score of ImageNet-pretrained ResNet-18 when transferred to multi-label prediction on CelebA, evaluating two selection methods for β : one optimized per attribute (**Micro Best**) and one using a globally optimal β (**Macro Best**) (**bold** values indicate cases where the metric remains the same under both selection methods). **The small performance gap between Micro Best and Macro Best demonstrates the stability of CT on more fine-grained downstream tasks.** Reported values are means over three runs for the first four attributes; the complete results for ResNet-18, ResNet-50, and ResNet-152, including standard deviations, are provided in Table 13, Table 14, Table 15, Table 16, Table 17 and Table 18.

(a) **Micro Best.**

Metric \ Attribute	Accuracy (%)	Balanced Accuracy (%)	F1 (%)
5 Shadow	91.54	65.91	44.16
Arch. Eyebrows	79.63	72.46	60.91
Attractive	79.44	79.47	80.15
Bags Un. Eyes	82.80	65.29	45.80

(b) **Macro Best.**

Metric \ Attribute	Accuracy (%)	Balanced Accuracy (%)	F1 (%)
5 Shadow	91.34	65.57	43.56
Arch. Eyebrows	79.34	71.97	60.14
Attractive	79.41	79.46	80.14
Bags Un. Eyes	82.80	65.12	45.48
Avg Rel Reduct (%)	0.16	0.37	0.83

4.4. Improving Generalization of Transformers

In this subsection, we demonstrate that CT is effective for transformers. Unlike models such as ResNets, where all layers adhere to the max-affine spline framework, transformers include attention layers that do not fit directly within this framework. Consequently, we lose strict theoretical guarantees when considering the end-to-end mapping of transformers. However, from a layer-wise perspective, the feed-forward layer combined with the activation function (if convex and piecewise-affine like ReLU) retains partial theoretical guarantees.

To show that CT remains effective even in cases with only partial theoretical guarantees, we modify the Swin Transformer (Liu et al., 2021) by replacing all GELU activations following the feed-forward layers with ReLU, enabling CT to be applied. The network is then pretrained on Imagenette (fastai, 2019) which is a subset of 10 easily classified classes from Imagenet and transferred to the 9 downstream datasets used in the **ImageNet-to-Multiple-Datasets Transfer** experiment in Section 4.1. Further details on the experimental setup are provided in Appendix D.5.

As shown in Table 6, CT improves the generalization of transformers even when partial theoretical guarantees are available. Specifically, CT achieves relative improvements of 2.43% on Swin-T and 3.33% on Swin-S, with average β values of 0.92 and 0.94, respectively, demonstrating CT’s

Table 5: Robust accuracy of ImageNet-pretrained ResNet-18, ResNet-50, and ResNet-152 under ℓ_2/ℓ_∞ adversarial attacks and common corruptions on CIFAR-10, CIFAR-100, and ImageNet (**bold** entries indicate improvement with CT). **CT consistently enhances robustness across models, datasets, and robustness settings, with β values close to 1**. Reported values are means over three runs; the complete results, including standard deviations, are provided in Table 19.

(a) **ResNet-18**. Avg rel improve: 11.76%. Avg β : 0.92.

Attack \ Dataset	ℓ_2			ℓ_∞			Corruption		
	ReLU (%)	+ CT (%)	(β)	ReLU (%)	+ CT (%)	(β)	ReLU (%)	+ CT (%)	(β)
CIFAR-10	53.67	53.67	1.00	11.17	14.93	0.90	77.73	77.73	1.00
CIFAR-100	24.30	25.50	0.92	4.47	6.90	0.92	51.81	51.95	0.94
ImageNet	23.37	23.37	1.00	0.00	7.00	0.89	33.11	33.32	0.92

(b) **ResNet-50**. Avg rel improve: 348.44%. Avg β : 0.95.

Attack \ Dataset	ℓ_2			ℓ_∞			Corruption		
	ReLU (%)	+ CT (%)	(β)	ReLU (%)	+ CT (%)	(β)	ReLU (%)	+ CT (%)	(β)
CIFAR-10	55.10	56.53	0.97	10.10	14.83	0.95	77.26	77.26	1.00
CIFAR-100	23.83	25.80	0.96	4.43	7.90	0.93	53.91	53.93	0.98
ImageNet	31.90	31.90	1.00	0.30	9.30	0.93	39.64	39.64	1.00

(c) **ResNet-152**. Avg rel improve: 498.41%. Avg β : 0.98.

Attack \ Dataset	ℓ_2			ℓ_∞			Corruption		
	ReLU (%)	+ CT (%)	(β)	ReLU (%)	+ CT (%)	(β)	ReLU (%)	+ CT (%)	(β)
CIFAR-10	56.27	56.27	1.00	11.47	15.00	0.99	78.82	78.83	0.99
CIFAR-100	27.90	28.23	0.98	5.40	7.70	0.99	56.12	56.12	1.00
ImageNet	42.50	42.50	1.00	0.30	13.53	0.97	45.47	45.47	0.99

effectiveness and efficiency once again.

Table 6: Accuracy of Imagenette-pretrained Swin-T and Swin-S (ReLU-based) when transferred to 9 downstream datasets (**bold** entries indicate improvement with CT). **CT consistently enhances generalization across models and datasets, with β values close to 1, demonstrating its effectiveness even with partial theoretical guarantees**. Reported values are means over three runs; the complete results, including standard deviations, are provided in Table 20.

Model \ Dataset	Swin-T			Swin-S		
	ReLU (%)	+ CT (%)	(β)	ReLU (%)	+ CT (%)	(β)
Arabic Characters	43.08	45.14	0.92	43.90	44.70	0.97
Arabic Digits	90.38	91.46	0.86	88.74	89.15	0.95
Beans	75.00	82.03	0.85	66.41	71.09	0.83
CUB-200-2011	6.97	7.02	0.93	6.40	6.70	0.94
DTD	21.51	21.70	0.93	20.59	21.28	0.94
Fashion MNIST	78.61	79.08	0.92	77.48	77.64	0.95
FGVC-Aircraft	8.13	8.31	0.98	7.12	7.70	0.96
Flowers102	23.77	24.19	0.94	22.29	23.01	0.95
Food101	17.35	17.41	0.98	17.11	17.29	0.95
Avg Rel Improve & β	Rel Improve (%)		(β)	Rel Improve (%)		(β)
	2.43		0.92	3.33		0.94

With CT’s effectiveness on improving the generalization of transformers demonstrated, even with partial theoretical guarantees, we now proceed to ablation studies to validate CT’s implementation.

4.5. Ablation Studies

To assess the impact of CT’s formulation, we conduct ablation studies on the two smoothing mechanisms introduced in Section 3.1: reparameterized Swish and SoftPlus. While each independently improves generalization and robustness, their combination proves the most effective.

We evaluate the effect of using only Swish or only SoftPlus in CT on the generalization experiment (transferring ImageNet-pretrained ResNets to 13 downstream tasks) and

the robustness experiment (evaluating on RobustBench). The results in Table 21 and Table 22 show that while both individual components provide improvements (0.23% and 2.96% for Swish and SoftPlus in generalization; 8.06% and 9.91% in robustness), the full CT formulation achieves the highest gains (3.46% in generalization; 11.76% in robustness). These findings align with our theoretical insights in Section 3.2, which show that combining both functions helps mitigate decision boundary drift.

In summary, we demonstrate the effectiveness and efficiency of CT in improving model generalization and robustness. Furthermore, our ablation studies empirically validate the theoretical findings in Section 3.2. Next, we summarize our results and discuss future directions.

5. Conclusion

In this paper, we propose a provable, training-free model steering technique, coined Curvature Tuning (CT), which enables adjustment of a model’s decision boundary curvature through a single parameter. We empirically demonstrate that CT enhances both the generalization and robustness of models across various scenarios.

CT offers an off-the-shelf solution that is agnostic to input modality, task type, or loss function. However, it does have a structural limitation: its applicability requires the use of specific activation functions such as ReLU, Swish, or SoftPlus due to its underlying formulation. While some current large-scale models, including DINOv2 and Llama3, do not adhere to this restriction, we have demonstrated that CT is effective on ReLU-based transformers. Moreover, a resurgence in the use of ReLU-based architectures (Mirzadeh et al., 2023) suggests that CT may soon become relevant

to an even broader range of state-of-the-art models with minimal effort.

Although CT and other Parameter-Efficient Fine-Tuning (PEFT) methods like LoRA cater to distinct fine-tuning needs, the theoretical foundations of CT have the potential to inspire further advancements in state-of-the-art techniques such as LoRA. We hope this work serves as a stepping stone for future research into efficient, principled approaches to post-training model steering.

Impact Statement

This paper presents work whose goal is to advance the field of Machine Learning. There are many potential societal consequences of our work, none which we feel must be specifically highlighted here.

References

- Balestrieri, R. and Baraniuk, R. G. From hard to soft: Understanding deep network nonlinearities via vector quantization and statistical inference. *arXiv preprint arXiv:1810.09274*, 2018.
- Balestrieri, R., Cosentino, R., Aazhang, B., and Baraniuk, R. The geometry of deep networks: Power diagram subdivision. *Advances in Neural Information Processing Systems*, 32, 2019.
- Balestrieri, R. et al. A spline theory of deep learning. In *International Conference on Machine Learning*, pp. 374–383. PMLR, 2018.
- Bossard, L., Guillaumin, M., and Van Gool, L. Food-101 – mining discriminative components with random forests. In *European Conference on Computer Vision*, 2014.
- Buitinck, L., Louppe, G., Blondel, M., Pedregosa, F., Mueller, A., Grisel, O., Niculae, V., Prettenhofer, P., Gramfort, A., Grobler, J., Layton, R., VanderPlas, J., Joly, A., Holt, B., and Varoquaux, G. API design for machine learning software: experiences from the scikit-learn project. In *ECML PKDD Workshop: Languages for Data Mining and Machine Learning*, pp. 108–122, 2013.
- Caron, M., Touvron, H., Misra, I., Jégou, H., Mairal, J., Bojanowski, P., and Joulin, A. Emerging properties in self-supervised vision transformers. In *Proceedings of the IEEE/CVF international conference on computer vision*, pp. 9650–9660, 2021.
- Chen, J., Zhang, A., Shi, X., Li, M., Smola, A., and Yang, D. Parameter-efficient fine-tuning design spaces. *arXiv preprint arXiv:2301.01821*, 2023.
- Chen, S., Tavallaie, O., Nazemi, N., Chen, X., and Zomaya, A. Y. Autorank: Mcda based rank personalization for lora-enabled distributed learning. *arXiv preprint arXiv:2412.15553*, 2024.
- Cimpoi, M., Maji, S., Kokkinos, I., Mohamed, S., and Vedaldi, A. Describing textures in the wild. In *Proceedings of the IEEE Conf. on Computer Vision and Pattern Recognition (CVPR)*, 2014.
- Croce, F., Andriushchenko, M., Sehwag, V., DeBenedetti, E., Flammarion, N., Chiang, M., Mittal, P., and Hein, M. Robustbench: a standardized adversarial robustness benchmark. *arXiv preprint arXiv:2010.09670*, 2020.
- Deng, J., Dong, W., Socher, R., Li, L.-J., Li, K., and Fei-Fei, L. Imagenet: A large-scale hierarchical image database. In *2009 IEEE conference on computer vision and pattern recognition*, pp. 248–255. Ieee, 2009.
- Dubey, A., Jauhri, A., Pandey, A., Kadian, A., Al-Dahle, A., Letman, A., Mathur, A., Schelten, A., Yang, A., Fan, A., et al. The llama 3 herd of models. *arXiv preprint arXiv:2407.21783*, 2024.
- El-Sawy, A., Hazem, E.-B., and Loey, M. Cnn for handwritten arabic digits recognition based on lenet-5. In *International conference on advanced intelligent systems and informatics*, pp. 566–575. Springer, 2016.
- El-Sawy, A., Loey, M., and El-Bakry, H. Arabic handwritten characters recognition using convolutional neural network. *WSEAS Transactions on Computer Research*, 5: 11–19, 2017.
- Everingham, M., Van Gool, L., Williams, C. K. I., Winn, J., and Zisserman, A. The PASCAL Visual Object Classes Challenge 2012 (VOC2012) Results. <http://www.pascal-network.org/challenges/VOC/voc2012/workshop/index.html>.
- fastai. Imagenette: A subset of 10 easily classified classes from imagenet. <https://github.com/fastai/imagenette>, 2019.
- Gao, C., Chen, K., Rao, J., Sun, B., Liu, R., Peng, D., Zhang, Y., Guo, X., Yang, J., and Subrahmanian, V. Higher layers need more lora experts. *arXiv preprint arXiv:2402.08562*, 2024.
- Guo, D., Rush, A. M., and Kim, Y. Parameter-efficient transfer learning with diff pruning. *arXiv preprint arXiv:2012.07463*, 2020.
- Han, Z., Gao, C., Liu, J., Zhang, J., and Zhang, S. Q. Parameter-efficient fine-tuning for large models: A comprehensive survey. *arXiv preprint arXiv:2403.14608*, 2024.
- Hayou, S., Ghosh, N., and Yu, B. The impact of initialization on lora finetuning dynamics. *arXiv preprint arXiv:2406.08447*, 2024.

- He, K., Zhang, X., Ren, S., and Sun, J. Deep residual learning for image recognition. In *Proceedings of the IEEE conference on computer vision and pattern recognition*, pp. 770–778, 2016.
- Hendrycks, D. and Dietterich, T. Benchmarking neural network robustness to common corruptions and perturbations. *arXiv preprint arXiv:1903.12261*, 2019.
- Houlsby, N., Giurgiu, A., Jastrzebski, S., Morrone, B., de Laroussilhe, Q., Gesmundo, A., Attariyan, M., and Gelly, S. Parameter-efficient transfer learning for nlp, 2019. URL <https://arxiv.org/abs/1902.00751>.
- Hu, E. J., Shen, Y., Wallis, P., Allen-Zhu, Z., Li, Y., Wang, S., Wang, L., and Chen, W. Lora: Low-rank adaptation of large language models, 2021. URL <https://arxiv.org/abs/2106.09685>.
- Jeddi, A., Shafiee, M. J., and Wong, A. A simple fine-tuning is all you need: Towards robust deep learning via adversarial fine-tuning. *arXiv preprint arXiv:2012.13628*, 2020.
- Kalajdziewski, D. A rank stabilization scaling factor for fine-tuning with lora. *arXiv preprint arXiv:2312.03732*, 2023.
- Kim, M. J., Pertsch, K., Karamcheti, S., Xiao, T., Balakrishna, A., Nair, S., Rafailov, R., Foster, E., Lam, G., Sanke, P., et al. Openvla: An open-source vision-language-action model. *arXiv preprint arXiv:2406.09246*, 2024.
- Krizhevsky, A., Hinton, G., et al. Learning multiple layers of features from tiny images. 2009.
- Li, X. L. and Liang, P. Prefix-tuning: Optimizing continuous prompts for generation. *arXiv preprint arXiv:2101.00190*, 2021.
- Liu, H., Tam, D., Muqeeth, M., Mohta, J., Huang, T., Bansal, M., and Raffel, C. A. Few-shot parameter-efficient fine-tuning is better and cheaper than in-context learning. *Advances in Neural Information Processing Systems*, 35: 1950–1965, 2022.
- Liu, Z., Luo, P., Wang, X., and Tang, X. Deep learning face attributes in the wild. In *Proceedings of International Conference on Computer Vision (ICCV)*, December 2015.
- Liu, Z., Lin, Y., Cao, Y., Hu, H., Wei, Y., Zhang, Z., Lin, S., and Guo, B. Swin transformer: Hierarchical vision transformer using shifted windows. In *Proceedings of the IEEE/CVF international conference on computer vision*, pp. 10012–10022, 2021.
- Maji, S., Rahtu, E., Kannala, J., Blaschko, M., and Vedaldi, A. Fine-grained visual classification of aircraft. *arXiv preprint arXiv:1306.5151*, 2013.
- Makerere AI Lab. Bean Disease Dataset, January 2020. URL <https://github.com/AI-Lab-Makerere/ibean/>.
- Mao, Y., Mathias, L., Hou, R., Almahairi, A., Ma, H., Han, J., Yih, W.-t., and Khabsa, M. Unipelt: A unified framework for parameter-efficient language model tuning. *arXiv preprint arXiv:2110.07577*, 2021.
- Matthey, L., Higgins, I., Hassabis, D., and Lerchner, A. dsprites: Disentanglement testing sprites dataset. <https://github.com/deepmind/dsprites-dataset/>, 2017.
- Mirzadeh, I., Alizadeh, K., Mehta, S., Del Mundo, C. C., Tuzel, O., Samei, G., Rastegari, M., and Farajtabar, M. Relu strikes back: Exploiting activation sparsity in large language models. *arXiv preprint arXiv:2310.04564*, 2023.
- Montufar, G. F., Pascanu, R., Cho, K., and Bengio, Y. On the number of linear regions of deep neural networks. *Advances in neural information processing systems*, 27, 2014.
- Nilsback, M.-E. and Zisserman, A. Automated flower classification over a large number of classes. In *2008 Sixth Indian conference on computer vision, graphics & image processing*, pp. 722–729. IEEE, 2008.
- Oquab, M., Darcet, T., Moutakanni, T., Vo, H., Szafraniec, M., Khalidov, V., Fernandez, P., Haziza, D., Massa, F., El Nouby, A., et al. Dinov2: Learning robust visual features without supervision. *arXiv preprint arXiv:2304.07193*, 2023.
- Paszke, A., Gross, S., Massa, F., Lerer, A., Bradbury, J., Chanan, G., Killeen, T., Lin, Z., Gimelshein, N., Antiga, L., et al. Pytorch: An imperative style, high-performance deep learning library. *Advances in neural information processing systems*, 32, 2019.
- Radford, A. Improving language understanding by generative pre-training. 2018.
- Radford, A., Kim, J. W., Hallacy, C., Ramesh, A., Goh, G., Agarwal, S., Sastry, G., Askell, A., Mishkin, P., Clark, J., Krueger, G., and Sutskever, I. Learning transferable visual models from natural language supervision, 2021. URL <https://arxiv.org/abs/2103.00020>.
- Ramachandran, P., Zoph, B., and Le, Q. V. Searching for activation functions. *arXiv preprint arXiv:1710.05941*, 2017.

- Valipour, M., Rezagholizadeh, M., Kobzyev, I., and Ghodsi, A. Dylora: Parameter efficient tuning of pre-trained models using dynamic search-free low-rank adaptation. *arXiv preprint arXiv:2210.07558*, 2022.
- Wah, C., Branson, S., Welinder, P., Perona, P., and Belongie, S. The caltech-ucsd birds-200-2011 dataset. Technical Report CNS-TR-2011-001, California Institute of Technology, 2011.
- Xiao, H., Rasul, K., and Vollgraf, R. Fashion-mnist: a novel image dataset for benchmarking machine learning algorithms. *arXiv preprint arXiv:1708.07747*, 2017.
- Yang, J., Shi, R., Wei, D., Liu, Z., Zhao, L., Ke, B., Pfister, H., and Ni, B. Medmnist v2-a large-scale lightweight benchmark for 2d and 3d biomedical image classification. *Scientific Data*, 10(1):41, 2023.
- Zhai, X., Mustafa, B., Kolesnikov, A., and Beyer, L. Sigmoid loss for language image pre-training. In *Proceedings of the IEEE/CVF International Conference on Computer Vision*, pp. 11975–11986, 2023.
- Zhao, H., Shi, J., Qi, X., Wang, X., and Jia, J. Pyramid scene parsing network. In *Proceedings of the IEEE conference on computer vision and pattern recognition*, pp. 2881–2890, 2017.

A. LoRA Fine-Tuning Parameter Counts

We provide details on the number of parameters tuned during fine-tuning of different ResNet models using LoRA with varying ranks, as shown in Table 7.

Table 7: Number of parameters to be tuned during fine-tuning of different ResNet models (total parameters shown in parentheses) using LoRA with varying ranks. **While LoRA with low ranks significantly reduces the number of parameters required for fine-tuning, these values still range from tens of thousands to over a million, reinforcing the need for CT in highly resource-constrained scenarios.**

Method \ Model	ResNet-18 (11.69M)	ResNet-50 (25.89M)	ResNet-152 (61.18M)
LoRA ($rank = 1$)	50K	14K	40K
LoRA ($rank = 2$)	8K	22K	64K
LoRA ($rank = 4$)	16K	38K	1.14M

B. Spline Theory

The spline theory of deep learning establishes that a large class of deep network (DN) layers can be modeled as MASOs. More precisely:

Theorem B.1. *Any DN layer comprising a linear operator (e.g., fully connected or convolutional layer) followed by a convex and piecewise affine non-linear operator (e.g., ReLU, leaky-ReLU, absolute value activation, max/average/channel pooling, maxout; with or without skip connections) is a MASO (Balestrierio et al., 2018).*

Consequently, a deep network (e.g., MLP, CNN, RNN, ResNet) composed of such linear operators and convex, piecewise affine non-linear operators is a composition of MASOs. However, it is important to note that the network as a whole is not a MASO but an ASO. In other words, conditioned on the input, such deep networks are equivalent to an affine transformation, but globally, the transformation is not convex.

C. Curvature Tuning (CT) Implementation

The following code provides a PyTorch implementation of CT. The CT class defines the new activation function as formulated in Equation (7), while the `replace_module` function searches for and replaces all ReLU activations in a network with CT.

```

import torch
from torch import nn

class CT(nn.Module):
    def __init__(self, beta=0, coeff=0.5, threshold=20, trainable=False):
        assert 0 <= beta < 1
        super().__init__()
        self.beta = nn.Parameter(torch.tensor(beta))
        self.beta.requires_grad_(trainable)
        self.coeff = coeff
        self.threshold = threshold

    def forward(self, x):
        beta = self.beta
        normal_ver = (
            self.coeff * torch.sigmoid(beta * x / (1 - beta)) * x +
            (1 - self.coeff) * torch.log(1 + torch.exp(x / (1 - beta))) * (1 - beta)
        )
        overflow_ver = (
            self.coeff * torch.sigmoid(beta * x / (1 - beta)) * x +
            (1 - self.coeff) * x
        )
        return torch.where(x / (1 - beta) <= self.threshold, normal_ver, overflow_ver)

class ReplacementMapping:
    def __init__(self, old_module, new_module, **kwargs):
        self.old_module = old_module
        self.new_module = new_module
        self.kwargs = kwargs

    def __call__(self, module):
        if isinstance(module, self.old_module):
            return self.new_module(**self.kwargs)
        return module

def replace_module(model, old_module=nn.ReLU, new_module=CT, **kwargs):
    if not isinstance(model, nn.Module):
        raise ValueError("Expected_model_to_be_an_instance_of_torch.nn.Module")

    replacement_mapping = ReplacementMapping(old_module, new_module, **kwargs)

    device = next(model.parameters(), torch.tensor([])).device # Handle models with no
    parameters

    for name, module in model.named_modules():
        if name == "":
            continue
        replacement = replacement_mapping(module).to(device)

        # Traverse module hierarchy to assign new module
        module_names = name.split(".")
        parent = model
        for name in module_names[:-1]:
            parent = getattr(parent, name)
        setattr(parent, module_names[-1], replacement)

    return model

```

D. Supplementary Experimental Details

D.1. Hardware

Our experiments are conducted with 8 RTX 3090 GPUs and 384GB of CPU memory. Since CT does not require backpropagation, the hardware demands for each experiment are minimal, allowing each experiment to fit on a single GPU.

D.2. Improving Generalization on Natural Image Datasets

This subsection provides additional details on the pretraining of our models used in the experiments in Section 4.1. We also present the complete results, including both the mean and standard deviation for ResNet-18, ResNet-50, and ResNet-152. Additionally, we provide visualizations of accuracy trends during the β search process and report further experiments validating the robustness of CT under different linear probing configurations.

Pretraining Details: For the **Cross-Dataset Transfer** experiment, we pretrain ResNet-18, ResNet-50, and ResNet-152 for 10 epochs on MNIST and 200 epochs on CIFAR-10 and CIFAR-100. For ImageNet, we use the pretrained weights provided by PyTorch (Paszke et al., 2019). Training is conducted using SGD with a learning rate of 0.1, momentum of 0.9, and weight decay of 5×10^{-4} . The batch size is set to 128, and cross-entropy loss is used.

A MultiStepLR (Paszke et al., 2019) scheduler with a decay factor of 0.2 is applied, with learning rate reductions at epochs 3, 6, and 9 for MNIST, and at epochs 60, 120, and 160 for CIFAR-10 and CIFAR-100.

For the **ImageNet-to-Multiple-Datasets Transfer** experiment, we use the pretrained weights provided by PyTorch.

Complete Experimental Results: The full results for the **Cross-Dataset Transfer** experiment are presented in Table 8, while those for the **ImageNet-to-Multiple-Datasets Transfer** experiment are shown in Table 9.

Table 8: Complete accuracy results of ResNet-18, ResNet-50, and ResNet-152 trained and tested across MNIST, CIFAR-10, CIFAR-100, and ImageNet (**bold** entries indicate improvement with CT). **CT consistently enhances generalization across models and datasets, with β values close to 1.** Reported values include means and standard deviations over three runs.

(a) **ResNet-18.** Avg rel improve: 1.68%. Avg β : 0.82.

Test	MNIST			CIFAR-10			CIFAR-100			ImageNet		
	ReLU (%)	+ CT (%)	(β)	ReLU (%)	+ CT (%)	(β)	ReLU (%)	+ CT (%)	(β)	ReLU (%)	+ CT (%)	(β)
MNIST	99.59 ± 0.00	99.59 ± 0.00	1.00 ± 0.00	86.08 ± 0.06	87.30 ± 0.17	0.92 ± 0.02	89.56 ± 0.09	92.85 ± 0.26	0.88 ± 0.00	98.10 ± 0.01	98.95 ± 0.01	0.68 ± 0.01
CIFAR-10	45.02 ± 0.03	47.68 ± 0.04	0.51 ± 0.01	94.87 ± 0.00	94.87 ± 0.00	1.00 ± 0.00	76.03 ± 0.04	76.90 ± 0.09	0.92 ± 0.02	85.68 ± 0.02	85.83 ± 0.04	0.93 ± 0.00
CIFAR-100	20.30 ± 0.10	21.80 ± 0.03	0.51 ± 0.01	35.21 ± 0.03	35.61 ± 0.24	0.97 ± 0.01	76.19 ± 0.00	76.21 ± 0.00	0.97 ± 0.00	63.15 ± 0.04	63.15 ± 0.04	1.00 ± 0.00
ImageNet	-	-	-	-	-	-	-	-	-	69.76 ± 0.00	69.84 ± 0.00	0.94 ± 0.00

(b) **ResNet-50.** Avg rel improve: 1.96%. Avg β : 0.89.

Train	MNIST			CIFAR-10			CIFAR-100			ImageNet		
	ReLU (%)	+ CT (%)	(β)	ReLU (%)	+ CT (%)	(β)	ReLU (%)	+ CT (%)	(β)	ReLU (%)	+ CT (%)	(β)
MNIST	98.77 ± 0.00	98.85 ± 0.00	0.89 ± 0.00	88.95 ± 0.05	89.04 ± 0.11	0.98 ± 0.01	94.61 ± 0.13	94.77 ± 0.07	0.97 ± 0.01	98.44 ± 0.02	98.64 ± 0.02	0.92 ± 0.01
CIFAR-10	38.47 ± 0.18	40.52 ± 0.04	0.60 ± 0.02	95.57 ± 0.00	95.57 ± 0.00	1.00 ± 0.00	83.54 ± 0.09	83.78 ± 0.10	0.95 ± 0.01	88.21 ± 0.02	88.47 ± 0.01	0.95 ± 0.01
CIFAR-100	12.99 ± 0.05	15.08 ± 0.02	0.60 ± 0.02	32.75 ± 0.16	33.54 ± 0.16	0.97 ± 0.01	78.02 ± 0.00	78.18 ± 0.00	0.98 ± 0.00	69.94 ± 0.06	70.13 ± 0.04	0.96 ± 0.01
ImageNet	-	-	-	-	-	-	-	-	-	76.15 ± 0.00	76.15 ± 0.00	1.00 ± 0.00

(c) **ResNet-152.** Avg rel improve: 0.40%. Avg β : 0.96.

Train	MNIST			CIFAR-10			CIFAR-100			ImageNet		
	ReLU (%)	+ CT (%)	(β)	ReLU (%)	+ CT (%)	(β)	ReLU (%)	+ CT (%)	(β)	ReLU (%)	+ CT (%)	(β)
MNIST	98.07 ± 0.00	98.07 ± 0.00	1.00 ± 0.00	80.45 ± 0.40	80.80 ± 0.28	0.98 ± 0.01	93.78 ± 0.15	93.97 ± 0.31	0.99 ± 0.01	98.66 ± 0.03	98.68 ± 0.03	0.95 ± 0.03
CIFAR-10	35.18 ± 0.07	35.70 ± 0.02	0.86 ± 0.01	95.28 ± 0.00	95.39 ± 0.00	0.99 ± 0.00	84.09 ± 0.16	84.10 ± 0.15	0.99 ± 0.01	90.27 ± 0.03	90.27 ± 0.03	1.00 ± 0.01
CIFAR-100	11.10 ± 0.04	11.39 ± 0.02	0.87 ± 0.01	26.58 ± 0.10	26.62 ± 0.05	0.99 ± 0.01	79.43 ± 0.00	79.58 ± 0.00	0.98 ± 0.00	72.95 ± 0.07	72.97 ± 0.05	1.00 ± 0.01
ImageNet	-	-	-	-	-	-	-	-	-	78.32 ± 0.00	78.32 ± 0.00	1.00 ± 0.00

Accuracy Trends During β Search: Accuracy trends observed during β search across multiple models and datasets are illustrated in Figure 3. As β increases, we observe a sharp rise in accuracy leading to a distinct peak, followed by a gradual decline as β continues to increase.

Robustness of CT to Linear Probing Configurations: We demonstrate that CT consistently improves the generalization performance of models across various linear probing settings.

The first setting we modify is the **regularization strength** of logistic regression (c) used to train the new classifier layer. Note that c here refers to the inverse of the regularization strength in logistic regression (as implemented in scikit-learn (Buitinck et al., 2013)), meaning that a larger value corresponds to a weaker regularization.

For the baseline described in Section 4.1, we set $c = 1$. To evaluate the impact of different regularization strengths, we also

Table 9: Complete accuracy results of ImageNet-pretrained ResNet-18, ResNet-50, and ResNet-152 when transferred to 9 downstream datasets (**bold** entries indicate improvement with CT). **CT consistently enhances generalization across models and datasets, with β values close to 1**. Reported values include means and standard deviations over three runs.

Model \ Dataset	ResNet-18			ResNet-50			ResNet-152		
	ReLU (%)	+ CT (%)	(β)	ReLU (%)	+ CT (%)	(β)	ReLU (%)	+ CT (%)	(β)
Arabic Characters	86.46 ± 0.00	92.11 ± 0.08	0.70 ± 0.00	88.02 ± 0.05	89.87 ± 0.06	0.91 ± 0.00	87.86 ± 0.05	88.70 ± 0.02	0.95 ± 0.00
Arabic Digits	97.92 ± 0.03	98.92 ± 0.01	0.72 ± 0.04	98.70 ± 0.02	98.79 ± 0.02	0.87 ± 0.00	98.23 ± 0.01	98.55 ± 0.03	0.95 ± 0.01
Beans	85.94 ± 0.00	94.53 ± 0.00	0.60 ± 0.00	93.75 ± 0.00	94.79 ± 0.45	0.94 ± 0.01	91.41 ± 0.00	93.75 ± 0.00	0.91 ± 0.00
CUB-200-2011	62.93 ± 0.00	63.60 ± 0.00	0.90 ± 0.00	66.09 ± 0.03	66.57 ± 0.05	0.93 ± 0.00	68.76 ± 0.00	69.74 ± 0.00	0.94 ± 0.00
DTD	64.38 ± 0.03	64.50 ± 0.03	0.92 ± 0.00	70.46 ± 0.08	70.82 ± 0.03	0.95 ± 0.01	70.48 ± 0.00	70.57 ± 0.06	0.98 ± 0.01
Fashion MNIST	88.54 ± 0.03	89.52 ± 0.01	0.87 ± 0.01	90.99 ± 0.03	91.30 ± 0.03	0.94 ± 0.01	90.48 ± 0.03	90.84 ± 0.04	0.93 ± 0.00
FGVC-Aircraft	43.75 ± 0.06	48.30 ± 0.04	0.77 ± 0.01	47.62 ± 0.06	51.09 ± 0.12	0.89 ± 0.00	49.93 ± 0.05	50.35 ± 0.03	0.94 ± 0.00
Flowers102	87.80 ± 0.01	87.96 ± 0.01	0.86 ± 0.00	89.56 ± 0.00	89.56 ± 0.00	1.00 ± 0.00	88.97 ± 0.00	89.15 ± 0.01	0.96 ± 0.00
Food101	59.70 ± 0.05	60.48 ± 0.02	0.89 ± 0.02	68.07 ± 0.05	68.13 ± 0.03	0.97 ± 0.01	70.95 ± 0.04	71.02 ± 0.01	0.99 ± 0.01
Avg Rel Improve & β	Rel Improve (%)		(β)	Rel Improve (%)		(β)	Rel Improve (%)		(β)
	3.53		0.80	1.36		0.93	0.77		0.95

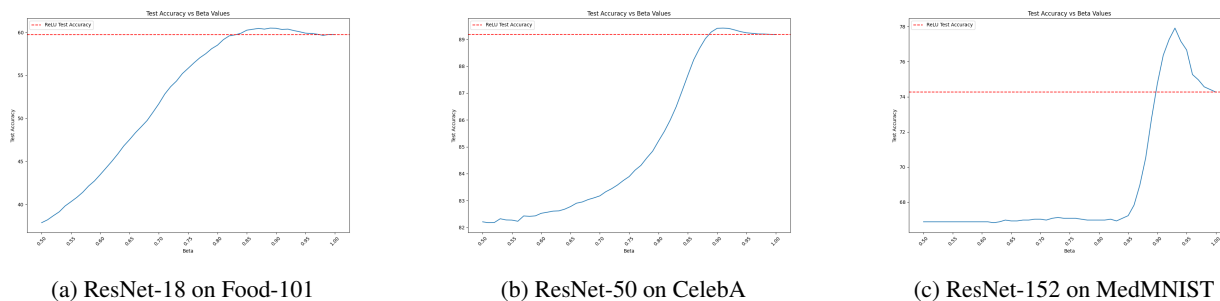


Figure 3: The accuracy trends during the β search process on various models and datasets. **A sharp increase leading to a distinct peak, followed by a gradual decline as β increases can be observed across models and datasets.**

test $c = 0.1$ (stronger regularization) and $c = 10$ (weaker regularization). The results, presented in Table 10, demonstrate that CT consistently enhances generalization performance across all tested regularization strengths.

The second setting we adjust is the **feature map** used for linear probing, specifically the number of layers contributing features to the linear classifier. The baseline configuration uses only the last layer’s features. Here, we test using features from the last 2 and 3 layers for linear probing. Due to the increased dimensionality of the combined feature maps, we train a fully connected classifier using Adam with a learning rate of 10^{-3} , optimizing for 30 epochs with cross-entropy loss. The results, shown in Table 11, indicate that CT consistently improves generalization performance regardless of the number of layers used for feature extraction.

D.3. Improving Generalization on Medical Image Datasets and Fine-grained Tasks

This subsection provides further details on the experimental setup for generalization in fine-grained tasks, as discussed in Section 4.2. We also present the complete results of the generalization experiments on medical image datasets and fine-grained tasks, along with a comparison of the per-attribute metrics for β selected using different methods.

Detailed Settings of Generalizing on Fine-grained Tasks: Since the ResNets are pretrained on single-label classification, when using them for more fine-grained downstream tasks, i.e. multi-label classification, regression and semantic segmentation, we need to adapt them specifically:

- **Multi-label Classification on CelebA:** For the multi-label classification task, since the output dimension differs from the original single label classification one, we use `MultiOutputClassifier` from scikit-learn (Buitinck et al., 2013) for linear probing, which trains 40 independent linear classifiers—one for each label.
- **Regression on dSprites:** For the regression task, we use the orientation of the shapes in dSprites as targets. Due to the large dataset size, we only sample 50,000 images for training and 10,000 for testing. For transfer learning, we use linear regression.

Table 10: Complete accuracy results of ResNet-18 trained and tested across MNIST, CIFAR-10, CIFAR-100, and ImageNet with varying regularization strengths (c) for logistic regression during linear probing (**bold** entries indicate improvement with CT). **CT consistently enhances generalization across different c values, with β values close to 1.** Reported values include means and standard deviations over three runs.

(a) $c = 0.1$. Avg rel improve: 1.37%. Avg β : 0.86.

Train \ Test	MNIST			CIFAR-10			CIFAR-100			ImageNet		
	ReLU (%)	+ CT (%)	(β)	ReLU (%)	+ CT (%)	(β)	ReLU (%)	+ CT (%)	(β)	ReLU (%)	+ CT (%)	(β)
MNIST	99.59 ± 0.00	99.59 ± 0.00	1.00 ± 0.00	75.36 ± 0.08	76.94 ± 0.15	0.93 ± 0.01	86.36 ± 0.04	90.21 ± 0.15	0.88 ± 0.00	97.99 ± 0.01	98.65 ± 0.01	0.71 ± 0.01
CIFAR-10	43.19 ± 0.04	44.32 ± 0.03	0.53 ± 0.01	94.87 ± 0.00	94.87 ± 0.00	1.00 ± 0.00	76.10 ± 0.22	77.04 ± 0.07	0.91 ± 0.01	86.10 ± 0.01	86.24 ± 0.00	0.96 ± 0.00
CIFAR-100	15.66 ± 0.03	16.42 ± 0.04	0.67 ± 0.01	24.02 ± 0.08	24.23 ± 0.07	0.98 ± 0.00	76.19 ± 0.00	76.21 ± 0.00	0.97 ± 0.00	66.94 ± 0.03	67.35 ± 0.04	0.94 ± 0.00
ImageNet	-	-	-	-	-	-	-	-	-	69.76 ± 0.00	69.84 ± 0.00	0.94 ± 0.00

(b) $c = 10$. Avg rel improve: 2.48%. Avg β : 0.83.

Train \ Test	MNIST			CIFAR-10			CIFAR-100			ImageNet		
	ReLU (%)	+ CT (%)	(β)	ReLU (%)	+ CT (%)	(β)	ReLU (%)	+ CT (%)	(β)	ReLU (%)	+ CT (%)	(β)
MNIST	99.59 ± 0.00	99.59 ± 0.00	1.00 ± 0.00	91.21 ± 0.12	92.04 ± 0.18	0.90 ± 0.01	89.94 ± 0.30	92.73 ± 0.51	0.88 ± 0.00	97.78 ± 0.02	98.99 ± 0.02	0.62 ± 0.01
CIFAR-10	44.72 ± 0.03	47.46 ± 0.06	0.53 ± 0.01	94.87 ± 0.00	94.87 ± 0.00	1.00 ± 0.00	75.92 ± 0.13	76.74 ± 0.04	0.91 ± 0.02	85.51 ± 0.03	85.69 ± 0.02	0.93 ± 0.00
CIFAR-100	19.89 ± 0.01	23.29 ± 0.02	0.51 ± 0.01	42.88 ± 0.10	43.54 ± 0.06	0.95 ± 0.01	76.19 ± 0.00	76.21 ± 0.00	0.97 ± 0.00	58.75 ± 0.02	59.27 ± 0.04	0.95 ± 0.01
ImageNet	-	-	-	-	-	-	-	-	-	69.76 ± 0.00	69.84 ± 0.00	0.94 ± 0.00

Table 11: Complete accuracy results of ResNet-18 trained and tested across MNIST, CIFAR-10, CIFAR-100, and ImageNet with varying number of layers from which features are extracted for linear probing (**bold** entries indicate improvement with CT). **CT consistently enhances generalization across different numbers of layers used, with β values close to 1.** Reported values include means and standard deviations over three runs.

(a) $layer = 2$. Avg rel improve: 2.76%. Avg β : 0.85.

Train \ Test	MNIST			CIFAR-10			CIFAR-100			ImageNet		
	ReLU (%)	+ CT (%)	(β)	ReLU (%)	+ CT (%)	(β)	ReLU (%)	+ CT (%)	(β)	ReLU (%)	+ CT (%)	(β)
MNIST	99.59 ± 0.00	99.59 ± 0.00	1.00 ± 0.00	93.07 ± 0.46	94.66 ± 0.21	0.92 ± 0.01	92.62 ± 1.06	95.00 ± 0.49	0.87 ± 0.01	99.15 ± 0.08	99.32 ± 0.02	0.77 ± 0.06
CIFAR-10	51.90 ± 0.21	54.49 ± 0.17	0.57 ± 0.01	94.87 ± 0.00	94.87 ± 0.00	1.00 ± 0.00	79.68 ± 0.17	80.37 ± 0.28	0.94 ± 0.03	87.14 ± 0.09	87.43 ± 0.03	0.94 ± 0.02
CIFAR-100	23.06 ± 0.32	25.50 ± 0.27	0.56 ± 0.06	40.31 ± 0.44	43.10 ± 0.40	0.93 ± 0.02	76.19 ± 0.00	76.21 ± 0.00	0.97 ± 0.00	63.41 ± 4.79	68.27 ± 0.24	0.99 ± 0.00
ImageNet	-	-	-	-	-	-	-	-	-	69.76 ± 0.00	69.84 ± 0.00	0.94 ± 0.00

(b) $layer = 3$. Avg rel improve: 2.38%. Avg β : 0.86.

Train \ Test	MNIST			CIFAR-10			CIFAR-100			ImageNet		
	ReLU (%)	+ CT (%)	(β)	ReLU (%)	+ CT (%)	(β)	ReLU (%)	+ CT (%)	(β)	ReLU (%)	+ CT (%)	(β)
MNIST	99.59 ± 0.00	99.59 ± 0.00	1.00 ± 0.00	98.16 ± 0.03	98.37 ± 0.09	0.90 ± 0.01	97.44 ± 0.19	97.28 ± 0.09	0.91 ± 0.03	99.26 ± 0.03	99.36 ± 0.01	0.85 ± 0.02
CIFAR-10	56.19 ± 0.48	58.46 ± 0.13	0.54 ± 0.04	94.87 ± 0.00	94.87 ± 0.00	1.00 ± 0.00	84.49 ± 0.11	84.82 ± 0.06	0.96 ± 0.03	88.71 ± 0.07	89.15 ± 0.01	0.94 ± 0.03
CIFAR-100	25.57 ± 0.15	28.03 ± 0.11	0.53 ± 0.02	56.92 ± 0.10	57.30 ± 0.25	0.97 ± 0.02	76.19 ± 0.00	76.21 ± 0.00	0.97 ± 0.00	60.69 ± 5.12	69.86 ± 0.23	0.94 ± 0.04
ImageNet	-	-	-	-	-	-	-	-	-	69.76 ± 0.00	69.84 ± 0.00	0.94 ± 0.00

- **Semantic Segmentation on VOC2012:** For the semantic segmentation task, we use an untrained PSPNet with a ResNet-50 encoder pretrained on ImageNet. We first apply CT to the encoder, then freeze it while training the remaining network (i.e. the decoder) on semantic segmentation, as this setup follows the common practice of using a pretrained ResNet as a fixed feature extractor for downstream tasks.

Complete Experimental Results: The full results for generalization on medical image datasets and fine-grained tasks are presented in Table 12. Additionally, the complete per-attribute metrics for β selection using the Micro Best and Macro Best strategies are provided in Table 13 and Table 14 for ResNet-18, Table 15 and Table 16 for ResNet-50, and Table 17 and Table 18 for ResNet-152.

D.4. Improving Robustness on Adversarial and Corrupted Data

This subsection provides details on the setup for robustness experiments and presents the complete results.

Detailed Settings of Robustness Experiments: To evaluate model robustness, we apply both adversarial attacks ℓ_2 and ℓ_∞ and common corruptions. For the ℓ_2 attack, we use an untargeted attack with $\ell_2 = 0.5$. For the ℓ_∞ attack, we use an untargeted attack with $\ell_\infty = \frac{8}{255}$. For corruption testing, we use CIFAR-C, CIFAR100-C, and ImageNet-C (Hendrycks & Dietterich, 2019).

Complete Experimental Results: The full results for the robustness experiments are presented in Table 19.

Table 12: Complete results of the performance of ImageNet-pretrained ResNet-18, ResNet-50, and ResNet-152 when transferred to challenging medical image datasets and fine-grained tasks (**bold** entries indicate improvement with CT). **CT consistently improves generalization across diverse datasets and tasks**. Reported values include means and standard deviations over three runs.

(a) **ResNet-18**. Avg rel improve: 2.69%. Avg β : 0.83.

Dataset	Metric	ReLU	+ CT	Rel Improve (%)	(β)
PathMNIST	Acc (%) \uparrow	86.21 \pm 0.00	87.27 \pm 0.01	1.23	0.81 \pm 0.00
OCTMNIST	Acc (%) \uparrow	65.47 \pm 0.06	69.00 \pm 0.26	5.40	0.80 \pm 0.04
DermaMNIST	Acc (%) \uparrow	73.44 \pm 0.03	77.74 \pm 0.08	5.86	0.80 \pm 0.01
CelebA	Mean Acc (%) \uparrow	87.88 \pm 0.00	88.44 \pm 0.00	0.64	0.75 \pm 0.01
dSprites	MSE \downarrow	4.09 \pm 0.01	4.08 \pm 0.00	0.33	0.98 \pm 0.00
VOC2012	mIoU \uparrow	-	-	-	-

(b) **ResNet-50**. Avg rel improve: 1.74%. Avg β : 0.86.

Dataset	Metric	ReLU	+ CT	Rel Improve (%)	(β)
PathMNIST	Acc (%) \uparrow	89.83 \pm 0.04	89.88 \pm 0.02	0.06	0.98 \pm 0.01
OCTMNIST	Acc (%) \uparrow	68.60 \pm 0.20	69.93 \pm 0.15	1.94	0.90 \pm 0.02
DermaMNIST	Acc (%) \uparrow	73.67 \pm 0.00	77.44 \pm 0.06	5.12	0.89 \pm 0.00
CelebA	Mean Acc (%) \uparrow	89.18 \pm 0.01	89.42 \pm 0.00	0.27	0.91 \pm 0.00
dSprites	MSE \downarrow	4.40 \pm 0.01	4.28 \pm 0.02	2.62	0.53 \pm 0.03
VOC2012	mIoU \uparrow	0.68 \pm 0.00	0.69 \pm 0.00	0.41	0.96 \pm 0.02

(c) **ResNet-152**. Avg rel improve: 4.22%. Avg β : 0.85.

Dataset	Metric	ReLU	+ CT	Rel Improve (%)	(β)
PathMNIST	Acc (%) \uparrow	90.15 \pm 0.04	90.75 \pm 0.06	0.66	0.92 \pm 0.00
OCTMNIST	Acc (%) \uparrow	70.23 \pm 0.15	71.03 \pm 0.06	1.14	0.98 \pm 0.00
DermaMNIST	Acc (%) \uparrow	74.39 \pm 0.12	77.92 \pm 0.07	4.75	0.93 \pm 0.00
CelebA	Mean Acc (%) \uparrow	89.16 \pm 0.02	89.40 \pm 0.02	0.27	0.92 \pm 0.01
dSprites	MSE \downarrow	4.46 \pm 0.02	3.82 \pm 0.02	14.27	0.52 \pm 0.02
VOC2012	mIoU \uparrow	-	-	-	-

D.5. Improving Generalization of Transformers

This subsection provides details on the pretraining of ReLU-based Swin transformers discussed in Section 4.4. It also includes the complete experimental results for Swin-T and Swin-S.

Pretraining Details: The pretraining of ReLU-based Swin transformers on Imagenette follows the same training configuration as used for ResNet-18/ResNet-50/ResNet-152 on CIFAR-10 and CIFAR-100, detailed in Appendix D.2. The training curves for Swin-T and Swin-S are shown in Figure 4.

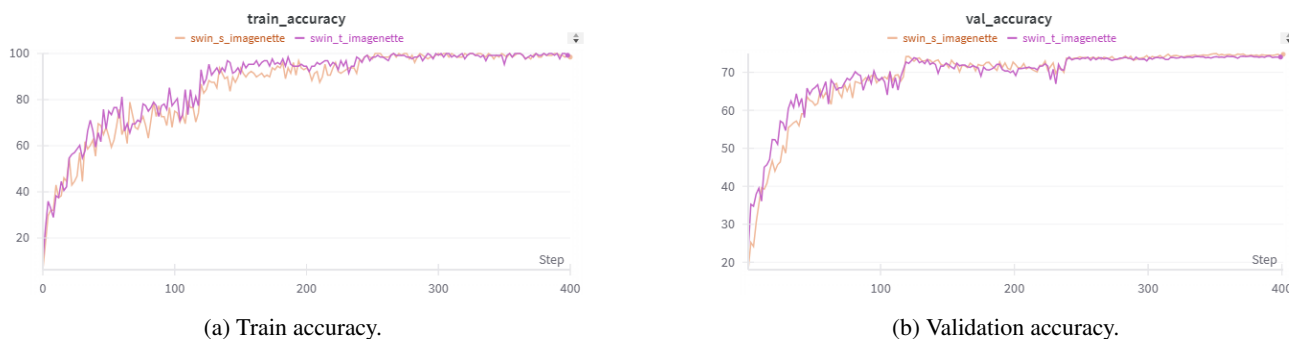


Figure 4: Training and validation accuracy curves for Swin-T and Swin-S.

Complete Experimental Results: The full results of the generalization experiments for Swin transformers are provided in Table 20.

D.6. Ablation Studies

This subsection presents the complete results of the ablation studies introduced in Section 4.5. Table 21 provides results for the generalization experiments, while Table 22 the robustness experiments.

Table 13: Per-attribute accuracy, balanced accuracy, and F1-score of ImageNet-pretrained ResNet-18 when transferred to multi-label prediction on CelebA, with the β of CT optimized per attribute (**Micro Best**). Reported values include means and standard deviations over three runs.

Attribute	Metric	Accuracy	Balanced Accuracy	F1
5 Shadow		91.54 ± 0.02	65.91 ± 0.01	44.16 ± 0.03
Arch. Eyebrows		79.63 ± 0.01	72.46 ± 0.02	60.91 ± 0.03
Attractive		79.44 ± 0.00	79.47 ± 0.00	80.15 ± 0.00
Bags Un. Eyes		82.80 ± 0.00	65.29 ± 0.01	45.80 ± 0.02
Bald		98.71 ± 0.00	80.49 ± 0.10	66.95 ± 0.18
Bangs		93.51 ± 0.01	84.83 ± 0.05	77.62 ± 0.06
Big Lips		69.53 ± 0.01	54.83 ± 0.03	20.94 ± 0.08
Big Nose		81.71 ± 0.02	66.77 ± 0.02	48.63 ± 0.05
Black Hair		86.41 ± 0.01	80.91 ± 0.01	73.35 ± 0.02
Blond Hair		94.92 ± 0.01	87.45 ± 0.04	80.20 ± 0.05
Blurry		96.05 ± 0.01	69.44 ± 0.06	50.48 ± 0.13
Brown Hair		85.89 ± 0.01	72.45 ± 0.02	56.72 ± 0.04
Bushy Eyebrows		89.14 ± 0.02	65.36 ± 0.03	44.23 ± 0.07
Chubby		95.09 ± 0.02	62.03 ± 0.06	34.98 ± 0.10
Double Chin		95.71 ± 0.02	61.68 ± 0.13	34.04 ± 0.34
Eyeglasses		98.91 ± 0.00	93.42 ± 0.03	91.15 ± 0.03
Goatee		96.07 ± 0.01	71.22 ± 0.07	50.55 ± 0.15
Gray Hair		97.83 ± 0.00	79.04 ± 0.11	63.38 ± 0.10
Heavy Makeup		88.01 ± 0.01	87.70 ± 0.01	85.32 ± 0.02
H. Cheekbones		81.45 ± 0.00	81.35 ± 0.00	80.39 ± 0.03
Male		93.80 ± 0.00	93.69 ± 0.00	92.08 ± 0.00
Mouth S. O.		80.45 ± 0.01	80.43 ± 0.01	79.90 ± 0.03
Mustache		96.23 ± 0.00	57.92 ± 0.00	25.01 ± 0.03
Narrow Eyes		85.90 ± 0.00	55.09 ± 0.01	19.17 ± 0.04
No Beard		91.32 ± 0.01	78.68 ± 0.01	95.00 ± 0.01
Oval Face		73.70 ± 0.00	60.37 ± 0.03	38.47 ± 0.05
Pale Skin		96.65 ± 0.02	67.28 ± 0.13	46.94 ± 0.32
Pointy Nose		73.96 ± 0.02	59.41 ± 0.01	35.86 ± 0.06
Reced. Hairline		91.87 ± 0.01	59.94 ± 0.02	30.94 ± 0.07
Rosy Cheeks		94.08 ± 0.01	67.31 ± 0.14	46.46 ± 0.21
Sideburns		96.59 ± 0.02	72.92 ± 0.09	55.83 ± 0.18
Smiling		84.71 ± 0.01	84.71 ± 0.01	84.60 ± 0.01
Straight Hair		81.62 ± 0.00	63.30 ± 0.01	42.02 ± 0.02
Wavy Hair		81.32 ± 0.02	77.06 ± 0.01	70.52 ± 0.02
Wear. Earrings		85.37 ± 0.00	71.29 ± 0.03	57.11 ± 0.04
Wear. Hat		98.76 ± 0.00	91.38 ± 0.00	85.00 ± 0.03
Wear. Lipstick		90.97 ± 0.00	91.03 ± 0.02	91.21 ± 0.01
Wear. Necklace		86.27 ± 0.00	51.21 ± 0.03	5.37 ± 0.09
Wear. Necktie		94.72 ± 0.01	71.55 ± 0.03	54.24 ± 0.04
Young		84.10 ± 0.01	72.23 ± 0.02	90.08 ± 0.00

Table 14: Per-attribute accuracy, balanced accuracy, and F1-score of ImageNet-pretrained ResNet-18 when transferred to multi-label prediction on CelebA, with the β of CT optimized globally for the highest mean accuracy across attributes (**Macro Best**) (**bold** values indicate cases where the metric remains the same under both Micro Best and Macro Best β). **The small performance gap between Micro Best and Macro Best demonstrates the stability of CT on more fine-grained downstream tasks.** Reported values include means and standard deviations over three runs.

Metric Attribute	Accuracy	Balanced Accuracy	F1
5 Shadow	91.34 ± 0.02	65.57 ± 0.03	43.56 ± 0.08
Arch. Eyebrows	79.34 ± 0.01	71.97 ± 0.02	60.14 ± 0.02
Attractive	79.41 ± 0.02	79.46 ± 0.02	80.14 ± 0.02
Bags Un. Eyes	82.80 ± 0.00	65.12 ± 0.00	45.48 ± 0.02
Bald	98.55 ± 0.01	78.56 ± 0.10	62.94 ± 0.22
Bangs	93.33 ± 0.01	84.34 ± 0.02	76.91 ± 0.03
Big Lips	69.28 ± 0.01	54.39 ± 0.02	19.54 ± 0.07
Big Nose	81.65 ± 0.01	66.64 ± 0.02	48.36 ± 0.04
Black Hair	85.16 ± 0.01	79.45 ± 0.01	71.27 ± 0.01
Blond Hair	94.85 ± 0.00	87.33 ± 0.01	79.94 ± 0.01
Blurry	95.89 ± 0.00	68.48 ± 0.13	48.10 ± 0.28
Brown Hair	85.47 ± 0.01	70.99 ± 0.05	54.57 ± 0.08
Bushy Eyebrows	89.14 ± 0.02	64.74 ± 0.03	42.94 ± 0.07
Chubby	95.04 ± 0.01	61.84 ± 0.12	34.49 ± 0.26
Double Chin	95.70 ± 0.00	61.16 ± 0.07	32.83 ± 0.20
Eyeglasses	98.90 ± 0.00	93.40 ± 0.02	91.15 ± 0.03
Goatee	95.94 ± 0.00	69.30 ± 0.05	47.66 ± 0.08
Gray Hair	97.77 ± 0.01	78.74 ± 0.19	62.72 ± 0.25
Heavy Makeup	87.76 ± 0.01	87.50 ± 0.01	85.07 ± 0.01
H. Cheekbones	81.38 ± 0.00	81.18 ± 0.01	80.23 ± 0.01
Male	93.41 ± 0.02	93.44 ± 0.00	91.76 ± 0.01
Mouth S. O.	80.44 ± 0.01	80.35 ± 0.04	79.90 ± 0.03
Mustache	96.23 ± 0.01	57.30 ± 0.13	23.51 ± 0.31
Narrow Eyes	85.88 ± 0.01	54.91 ± 0.02	18.67 ± 0.04
No Beard	90.95 ± 0.01	77.63 ± 0.04	94.83 ± 0.01
Oval Face	73.63 ± 0.01	60.08 ± 0.02	37.76 ± 0.05
Pale Skin	96.46 ± 0.01	63.13 ± 0.06	38.83 ± 0.14
Pointy Nose	73.83 ± 0.00	58.86 ± 0.05	34.57 ± 0.11
Reced. Hairline	91.68 ± 0.01	59.12 ± 0.05	28.97 ± 0.12
Rosy Cheeks	93.91 ± 0.01	66.99 ± 0.09	45.60 ± 0.18
Sideburns	96.54 ± 0.01	71.33 ± 0.06	53.65 ± 0.04
Smiling	84.31 ± 0.01	84.15 ± 0.01	84.10 ± 0.02
Straight Hair	81.26 ± 0.01	62.67 ± 0.01	40.69 ± 0.02
Wavy Hair	80.98 ± 0.03	76.92 ± 0.02	70.32 ± 0.03
Wear. Earrings	85.26 ± 0.01	71.15 ± 0.01	56.84 ± 0.02
Wear. Hat	98.73 ± 0.00	90.19 ± 0.07	84.03 ± 0.11
Wear. Lipstick	90.92 ± 0.00	91.03 ± 0.02	91.19 ± 0.02
Wear. Necklace	86.05 ± 0.01	51.02 ± 0.04	4.79 ± 0.14
Wear. Necktie	94.38 ± 0.02	69.16 ± 0.07	50.14 ± 0.16
Young	84.03 ± 0.01	72.13 ± 0.01	90.04 ± 0.00
Avg Rel Reduction (%)	0.21	0.96	2.81

Table 15: Per-attribute accuracy, balanced accuracy, and F1-score of ImageNet-pretrained ResNet-50 when transferred to multi-label prediction on CelebA, with the β of CT optimized per attribute (**Micro Best**). Reported values include means and standard deviations over three runs.

Metric	Accuracy	Balanced Accuracy	F1
5 Shadow	92.32 ± 0.02	71.34 ± 0.12	53.97 ± 0.21
Arched Eyebrows	80.61 ± 0.06	74.22 ± 0.10	63.54 ± 0.14
Attractive	80.68 ± 0.02	80.71 ± 0.02	81.20 ± 0.01
Bags Under Eyes	83.11 ± 0.02	67.27 ± 0.03	49.37 ± 0.06
Bald	98.73 ± 0.01	81.58 ± 0.30	67.90 ± 0.20
Bangs	94.79 ± 0.01	87.96 ± 0.03	82.34 ± 0.05
Big Lips	70.05 ± 0.01	56.10 ± 0.02	25.67 ± 0.09
Big Nose	82.52 ± 0.03	69.63 ± 0.03	53.41 ± 0.06
Black Hair	88.01 ± 0.02	83.17 ± 0.04	76.68 ± 0.05
Blond Hair	95.10 ± 0.02	88.07 ± 0.05	81.00 ± 0.06
Blurry	96.05 ± 0.02	71.40 ± 0.09	52.88 ± 0.11
Brown Hair	85.89 ± 0.03	74.11 ± 0.04	58.67 ± 0.07
Bushy Eyebrows	89.42 ± 0.00	67.66 ± 0.04	48.40 ± 0.06
Chubby	95.23 ± 0.02	65.82 ± 0.06	42.21 ± 0.13
Double Chin	96.00 ± 0.01	64.78 ± 0.09	41.04 ± 0.19
Eyeglasses	99.18 ± 0.00	95.01 ± 0.03	93.41 ± 0.04
Goatee	96.33 ± 0.01	75.45 ± 0.05	56.72 ± 0.10
Gray Hair	98.01 ± 0.01	80.34 ± 0.13	66.27 ± 0.16
Heavy Makeup	88.85 ± 0.01	88.66 ± 0.01	86.42 ± 0.02
High Cheekbones	84.00 ± 0.05	83.91 ± 0.05	83.05 ± 0.05
Male	95.74 ± 0.02	95.50 ± 0.02	94.49 ± 0.02
Mouth Slightly Open	86.89 ± 0.02	86.87 ± 0.02	86.48 ± 0.02
Mustache	96.35 ± 0.02	60.56 ± 0.17	31.46 ± 0.30
Narrow Eyes	86.34 ± 0.02	57.40 ± 0.08	26.10 ± 0.24
No Beard	93.19 ± 0.01	83.34 ± 0.07	96.06 ± 0.00
Oval Face	74.31 ± 0.03	62.11 ± 0.03	42.61 ± 0.07
Pale Skin	96.59 ± 0.02	69.14 ± 0.05	48.66 ± 0.05
Pointy Nose	74.84 ± 0.02	61.83 ± 0.03	41.67 ± 0.05
Receding Hairline	92.69 ± 0.01	65.82 ± 0.04	43.72 ± 0.05
Rosy Cheeks	94.44 ± 0.02	70.59 ± 0.04	52.41 ± 0.04
Sideburns	97.04 ± 0.02	77.68 ± 0.11	63.88 ± 0.14
Smiling	88.23 ± 0.00	88.23 ± 0.00	88.12 ± 0.00
Straight Hair	82.77 ± 0.01	67.49 ± 0.05	50.05 ± 0.09
Wavy Hair	83.21 ± 0.01	79.41 ± 0.02	73.95 ± 0.02
Wearing Earrings	86.97 ± 0.03	75.77 ± 0.04	64.25 ± 0.08
Wearing Hat	98.94 ± 0.00	93.44 ± 0.03	87.36 ± 0.06
Wearing Lipstick	92.23 ± 0.03	92.26 ± 0.03	92.48 ± 0.03
Wearing Necklace	86.30 ± 0.01	52.81 ± 0.02	11.70 ± 0.14
Wearing Necktie	95.28 ± 0.00	76.54 ± 0.05	61.91 ± 0.06
Young	85.85 ± 0.01	75.81 ± 0.02	91.07 ± 0.01

Table 16: Per-attribute accuracy, balanced accuracy, and F1-score of ImageNet-pretrained ResNet-50 when transferred to multi-label prediction on CelebA, with the β of CT optimized globally for the highest mean accuracy across attributes (**Macro Best**) (**bold** values indicate cases where the metric remains the same under both Micro Best and Macro Best β). **The small performance gap between Micro Best and Macro Best demonstrates the stability of CT on more fine-grained downstream tasks.** Reported values include means and standard deviations over three runs.

Metric	Accuracy	Balanced Accuracy	F1
5 Shadow	92.24 ± 0.01	70.98 ± 0.06	53.47 ± 0.08
Arched Eyebrows	79.49 ± 0.02	72.08 ± 0.04	60.34 ± 0.07
Attractive	80.68 ± 0.02	80.57 ± 0.02	81.05 ± 0.02
Bags Under Eyes	83.11 ± 0.02	67.27 ± 0.04	49.36 ± 0.06
Bald	98.72 ± 0.00	81.18 ± 0.25	67.42 ± 0.36
Bangs	94.52 ± 0.00	87.58 ± 0.01	81.53 ± 0.01
Big Lips	70.03 ± 0.01	56.04 ± 0.03	25.48 ± 0.11
Big Nose	82.52 ± 0.03	69.48 ± 0.03	53.18 ± 0.05
Black Hair	87.58 ± 0.02	83.12 ± 0.04	76.57 ± 0.07
Blond Hair	95.10 ± 0.02	87.68 ± 0.02	80.42 ± 0.03
Blurry	95.96 ± 0.01	69.99 ± 0.06	50.43 ± 0.09
Brown Hair	85.59 ± 0.02	72.95 ± 0.06	56.99 ± 0.09
Bushy Eyebrows	88.96 ± 0.01	66.35 ± 0.02	45.76 ± 0.05
Chubby	95.23 ± 0.02	64.93 ± 0.06	40.46 ± 0.11
Double Chin	95.86 ± 0.00	64.08 ± 0.00	38.95 ± 0.07
Eyeglasses	99.06 ± 0.00	94.81 ± 0.07	92.96 ± 0.11
Goatee	96.19 ± 0.02	74.74 ± 0.07	55.57 ± 0.08
Gray Hair	97.94 ± 0.01	80.34 ± 0.13	66.27 ± 0.16
Heavy Makeup	88.76 ± 0.01	88.66 ± 0.01	86.42 ± 0.02
High Cheekbones	83.92 ± 0.03	83.82 ± 0.02	83.03 ± 0.02
Male	95.62 ± 0.02	95.50 ± 0.02	94.49 ± 0.02
Mouth Slightly Open	86.34 ± 0.03	85.90 ± 0.00	85.50 ± 0.01
Mustache	96.18 ± 0.01	60.41 ± 0.04	30.68 ± 0.16
Narrow Eyes	85.89 ± 0.01	55.31 ± 0.02	20.08 ± 0.05
No Beard	92.97 ± 0.03	83.04 ± 0.09	96.02 ± 0.01
Oval Face	74.01 ± 0.02	61.74 ± 0.01	41.92 ± 0.03
Pale Skin	96.50 ± 0.01	68.31 ± 0.09	47.87 ± 0.11
Pointy Nose	74.84 ± 0.01	61.61 ± 0.04	41.22 ± 0.09
Receding Hairline	92.59 ± 0.01	65.82 ± 0.04	43.72 ± 0.05
Rosy Cheeks	94.32 ± 0.00	69.86 ± 0.09	50.94 ± 0.18
Sideburns	96.91 ± 0.02	76.67 ± 0.22	62.11 ± 0.41
Smiling	88.23 ± 0.00	88.15 ± 0.03	88.04 ± 0.03
Straight Hair	82.72 ± 0.02	67.25 ± 0.05	49.58 ± 0.08
Wavy Hair	82.91 ± 0.02	79.34 ± 0.02	73.85 ± 0.03
Wearing Earrings	86.80 ± 0.01	75.40 ± 0.02	63.68 ± 0.04
Wearing Hat	98.88 ± 0.01	92.99 ± 0.12	86.57 ± 0.09
Wearing Lipstick	92.22 ± 0.01	92.26 ± 0.03	92.48 ± 0.03
Wearing Necklace	86.25 ± 0.01	52.81 ± 0.02	11.68 ± 0.08
Wearing Necktie	95.27 ± 0.00	76.41 ± 0.20	61.73 ± 0.39
Young	85.77 ± 0.04	75.71 ± 0.02	91.04 ± 0.01
Avg Rel Reduction (%)	0.18	0.65	1.87

Table 17: Per-attribute accuracy, balanced accuracy, and F1-score of ImageNet-pretrained ResNet-152 when transferred to multi-label prediction on CelebA, with the β of CT optimized per attribute (**Micro Best**). Reported values include means and standard deviations over three runs.

Attribute	Metric	Accuracy	Balanced Accuracy	F1
5 Shadow		92.22 ± 0.05	70.68 ± 0.32	52.89 ± 0.55
Arch. Eyebrows		79.90 ± 0.29	72.86 ± 0.37	61.54 ± 0.57
Attractive		80.68 ± 0.10	80.71 ± 0.10	81.17 ± 0.09
Bags Un. Eyes		83.30 ± 0.14	67.64 ± 0.25	50.06 ± 0.47
Bald		98.69 ± 0.03	79.25 ± 0.98	65.60 ± 1.06
Bangs		94.43 ± 0.01	87.16 ± 0.10	81.08 ± 0.08
Big Lips		70.15 ± 0.14	56.21 ± 0.10	25.95 ± 0.29
Big Nose		82.62 ± 0.07	69.63 ± 0.08	53.46 ± 0.15
Black Hair		88.07 ± 0.11	83.39 ± 0.21	76.91 ± 0.27
Blond Hair		95.01 ± 0.03	87.75 ± 0.05	80.59 ± 0.09
Blurry		96.09 ± 0.08	71.55 ± 1.06	53.15 ± 1.87
Brown Hair		86.44 ± 0.43	75.15 ± 1.21	60.29 ± 1.92
Bushy Eyebrows		89.50 ± 0.35	67.69 ± 0.95	48.56 ± 1.98
Chubby		95.10 ± 0.04	65.00 ± 0.53	40.24 ± 0.33
Double Chin		95.84 ± 0.02	64.87 ± 0.56	40.32 ± 0.93
Eyeglasses		99.04 ± 0.09	94.56 ± 0.34	92.35 ± 0.70
Goatee		96.41 ± 0.07	75.42 ± 0.17	57.21 ± 0.59
Gray Hair		97.89 ± 0.05	80.04 ± 0.15	64.72 ± 0.54
Heavy Makeup		88.97 ± 0.08	88.72 ± 0.03	86.51 ± 0.06
H. Cheekbones		84.04 ± 0.10	83.95 ± 0.09	83.11 ± 0.06
Male		95.56 ± 0.01	95.34 ± 0.00	94.26 ± 0.00
Mouth S. O.		84.97 ± 0.67	84.94 ± 0.68	84.44 ± 0.76
Mustache		96.30 ± 0.09	61.01 ± 0.27	32.10 ± 0.45
Narrow Eyes		86.04 ± 0.10	56.27 ± 0.70	22.85 ± 2.02
No Beard		93.00 ± 0.15	82.94 ± 0.17	95.95 ± 0.09
Oval Face		74.29 ± 0.18	62.11 ± 0.25	42.63 ± 0.47
Pale Skin		96.71 ± 0.11	69.98 ± 1.09	51.08 ± 2.16
Pointy Nose		74.95 ± 0.08	61.83 ± 0.06	41.59 ± 0.11
Reced. Hairline		92.42 ± 0.20	64.20 ± 1.15	40.32 ± 2.44
Rosy Cheeks		94.34 ± 0.06	70.34 ± 0.05	51.73 ± 0.11
Sideburns		96.98 ± 0.01	76.50 ± 0.58	62.38 ± 0.56
Smiling		87.93 ± 0.16	87.93 ± 0.16	87.85 ± 0.15
Straight Hair		82.49 ± 0.03	66.92 ± 0.21	48.98 ± 0.37
Wavy Hair		83.08 ± 0.02	79.22 ± 0.03	73.68 ± 0.04
Wear. Earrings		86.83 ± 0.14	75.37 ± 0.17	63.61 ± 0.33
Wear. Hat		98.95 ± 0.04	93.47 ± 0.22	87.52 ± 0.48
Wear. Lipstick		91.87 ± 0.23	91.91 ± 0.22	92.10 ± 0.24
Wear. Necklace		86.28 ± 0.01	52.80 ± 0.03	11.82 ± 0.10
Wear. Necktie		95.36 ± 0.06	77.28 ± 0.59	62.92 ± 0.81
Young		85.79 ± 0.02	75.89 ± 0.08	91.02 ± 0.02

Table 18: Per-attribute accuracy, balanced accuracy, and F1-score of ImageNet-pretrained ResNet-152 when transferred to multi-label prediction on CelebA, with the β of CT optimized globally for the highest mean accuracy across attributes (**Macro Best**) (**bold** values indicate cases where the metric remains the same under both Micro Best and Macro Best β). **The small performance gap between Micro Best and Macro Best demonstrates the stability of CT on more fine-grained downstream tasks.** Reported values include means and standard deviations over three runs.

Metric \ Attribute	Accuracy	Balanced Accuracy	F1
5 Shadow	92.18 ± 0.10	70.58 ± 0.64	52.64 ± 1.14
Arch. Eyebrows	79.70 ± 0.23	72.44 ± 0.51	60.86 ± 0.78
Attractive	80.68 ± 0.10	80.65 ± 0.07	81.12 ± 0.05
Bags Un. Eyes	83.30 ± 0.14	67.49 ± 0.24	49.77 ± 0.43
Bald	98.58 ± 0.09	78.18 ± 1.97	63.82 ± 2.62
Bangs	94.39 ± 0.10	87.16 ± 0.10	81.08 ± 0.08
Big Lips	70.11 ± 0.06	56.16 ± 0.19	25.62 ± 0.50
Big Nose	82.62 ± 0.07	69.35 ± 0.14	52.91 ± 0.22
Black Hair	88.07 ± 0.11	83.32 ± 0.14	76.79 ± 0.15
Blond Hair	95.01 ± 0.03	87.75 ± 0.05	80.56 ± 0.11
Blurry	96.06 ± 0.10	71.19 ± 0.88	52.38 ± 1.83
Brown Hair	86.30 ± 0.53	74.96 ± 1.22	60.02 ± 1.87
Bushy Eyebrows	89.50 ± 0.35	67.24 ± 0.98	47.59 ± 2.12
Chubby	95.10 ± 0.04	64.92 ± 0.11	40.24 ± 0.33
Double Chin	95.84 ± 0.01	64.67 ± 0.43	39.71 ± 0.70
Eyeglasses	98.96 ± 0.10	94.38 ± 0.41	92.20 ± 0.67
Goatee	96.29 ± 0.04	75.13 ± 0.19	56.80 ± 0.22
Gray Hair	97.85 ± 0.12	80.00 ± 0.09	64.72 ± 0.54
Heavy Makeup	88.97 ± 0.08	88.57 ± 0.07	86.35 ± 0.09
H. Cheekbones	84.04 ± 0.10	83.77 ± 0.18	82.96 ± 0.18
Male	95.38 ± 0.24	95.25 ± 0.12	94.12 ± 0.20
Mouth S. O.	84.97 ± 0.67	84.62 ± 0.51	84.17 ± 0.52
Mustache	96.24 ± 0.01	60.15 ± 0.15	30.39 ± 0.50
Narrow Eyes	85.98 ± 0.22	55.54 ± 0.33	20.75 ± 0.97
No Beard	92.80 ± 0.24	82.82 ± 0.22	95.92 ± 0.05
Oval Face	74.29 ± 0.18	62.04 ± 0.21	42.56 ± 0.42
Pale Skin	96.71 ± 0.11	69.80 ± 1.01	50.41 ± 1.76
Pointy Nose	74.74 ± 0.02	61.52 ± 0.02	41.15 ± 0.16
Reced. Hairline	92.42 ± 0.20	64.04 ± 1.03	39.85 ± 2.23
Rosy Cheeks	94.28 ± 0.02	69.58 ± 0.05	50.24 ± 0.20
Sideburns	96.82 ± 0.08	76.50 ± 0.58	62.38 ± 0.56
Smiling	87.85 ± 0.21	87.93 ± 0.16	87.85 ± 0.15
Straight Hair	82.49 ± 0.03	66.83 ± 0.15	48.80 ± 0.25
Wavy Hair	82.82 ± 0.24	79.10 ± 0.21	73.50 ± 0.30
Wear. Earrings	86.78 ± 0.01	75.37 ± 0.17	63.61 ± 0.33
Wear. Hat	98.89 ± 0.02	93.47 ± 0.22	87.52 ± 0.48
Wear. Lipstick	91.87 ± 0.23	91.80 ± 0.24	92.01 ± 0.24
Wear. Necklace	86.17 ± 0.09	52.70 ± 0.06	11.44 ± 0.17
Wear. Necktie	95.34 ± 0.01	77.19 ± 0.50	62.83 ± 0.71
Young	85.62 ± 0.11	75.89 ± 0.08	91.02 ± 0.02
Avg Rel Reduction (%)	0.07	0.30	1.00

Table 19: Complete robust accuracy results of ImageNet-pretrained ResNet-18, ResNet-50, and ResNet-152 under ℓ_2/ℓ_∞ adversarial attacks and common corruptions on CIFAR-10, CIFAR-100, and ImageNet (**bold** entries indicate improvement with CT). **CT consistently enhances robustness across models, datasets, and robustness settings, with β values close to 1.** Reported values include means and standard deviations over three runs.

(a) ResNet-18. Avg rel improve: 11.76%. Avg β : 0.92.

Dataset	Attack	ℓ_2			ℓ_∞			Corruption		
		ReLU (%)	+ CT (%)	(β)	ReLU (%)	+ CT (%)	(β)	ReLU (%)	+ CT (%)	(β)
CIFAR-10		53.67 ± 0.32	53.67 ± 0.32	1.00 ± 0.00	11.17 ± 0.06	14.93 ± 0.06	0.90 ± 0.00	77.73 ± 0.00	77.73 ± 0.00	1.00 ± 0.00
CIFAR-100		24.30 ± 0.10	25.50 ± 0.00	0.92 ± 0.00	4.47 ± 0.06	6.90 ± 0.00	0.92 ± 0.00	51.81 ± 0.00	51.95 ± 0.00	0.94 ± 0.00
ImageNet		23.37 ± 0.06	23.37 ± 0.06	1.00 ± 0.00	0.00 ± 0.00	7.00 ± 0.10	0.89 ± 0.00	33.11 ± 0.00	33.32 ± 0.00	0.92 ± 0.00

(b) ResNet-50. Avg rel improve: 348.44%. Avg β : 0.95.

Dataset	Attack	ℓ_2			ℓ_∞			Corruption		
		ReLU (%)	+ CT (%)	(β)	ReLU (%)	+ CT (%)	(β)	ReLU (%)	+ CT (%)	(β)
CIFAR-10		55.10 ± 0.10	56.53 ± 0.21	0.97 ± 0.00	10.10 ± 0.17	14.83 ± 0.06	0.95 ± 0.00	77.26 ± 0.00	77.26 ± 0.00	1.00 ± 0.00
CIFAR-100		23.83 ± 0.06	25.80 ± 0.20	0.96 ± 0.00	4.43 ± 0.06	7.90 ± 0.00	0.93 ± 0.00	53.91 ± 0.00	53.93 ± 0.00	0.98 ± 0.00
ImageNet		31.90 ± 0.00	31.90 ± 0.00	1.00 ± 0.00	0.30 ± 0.00	9.30 ± 0.17	0.93 ± 0.00	39.64 ± 0.00	39.64 ± 0.00	1.00 ± 0.00

(c) ResNet-152. Avg rel improve: 498.41%. Avg β : 0.98.

Dataset	Attack	ℓ_2			ℓ_∞			Corruption		
		ReLU (%)	+ CT (%)	(β)	ReLU (%)	+ CT (%)	(β)	ReLU (%)	+ CT (%)	(β)
CIFAR-10		56.27 ± 0.23	56.27 ± 0.23	1.00 ± 0.00	11.47 ± 0.06	15.00 ± 0.20	0.99 ± 0.00	78.82 ± 0.00	78.83 ± 0.00	0.99 ± 0.00
CIFAR-100		27.90 ± 0.10	28.23 ± 0.12	0.98 ± 0.00	5.40 ± 0.00	7.70 ± 0.17	0.99 ± 0.00	56.12 ± 0.00	56.12 ± 0.00	1.00 ± 0.00
ImageNet		42.50 ± 0.00	42.50 ± 0.00	1.00 ± 0.00	0.30 ± 0.00	13.53 ± 0.06	0.97 ± 0.01	45.47 ± 0.00	45.47 ± 0.00	0.99 ± 0.00

Table 20: Complete accuracy results of Imagenette-pretrained Swin-T and Swin-S (ReLU-based) when transferred to 9 downstream datasets (**bold** entries indicate improvement with CT). **CT consistently enhances generalization across models and datasets, with β values close to 1, demonstrating its effectiveness even with partial theoretical guarantees.** Reported values include means and standard deviations over three runs.

Dataset	Model	Swin-T			Swin-S		
		ReLU (%)	+ CT (%)	(β)	ReLU (%)	+ CT (%)	(β)
Arabic Characters		43.08 ± 0.06	45.14 ± 0.07	0.92 ± 0.00	43.90 ± 0.08	44.70 ± 0.09	0.97 ± 0.00
Arabic Digits		90.38 ± 0.04	91.46 ± 0.03	0.86 ± 0.01	88.74 ± 0.01	89.15 ± 0.06	0.95 ± 0.01
Beans		75.00 ± 0.00	82.03 ± 0.00	0.85 ± 0.00	66.41 ± 0.00	71.09 ± 0.00	0.83 ± 0.00
CUB-200-2011		6.97 ± 0.00	7.02 ± 0.00	0.93 ± 0.01	6.40 ± 0.00	6.70 ± 0.00	0.94 ± 0.00
DTD		21.51 ± 0.06	21.70 ± 0.00	0.93 ± 0.00	20.59 ± 0.00	21.28 ± 0.00	0.94 ± 0.00
Fashion MNIST		78.61 ± 0.02	79.08 ± 0.01	0.92 ± 0.02	77.48 ± 0.01	77.64 ± 0.05	0.95 ± 0.00
FGVC-Aircraft		8.13 ± 0.00	8.31 ± 0.00	0.98 ± 0.00	7.12 ± 0.07	7.70 ± 0.02	0.96 ± 0.00
Flowers102		23.77 ± 0.02	24.19 ± 0.07	0.94 ± 0.00	22.29 ± 0.02	23.01 ± 0.05	0.95 ± 0.00
Food101		17.35 ± 0.02	17.41 ± 0.04	0.98 ± 0.01	17.11 ± 0.01	17.29 ± 0.03	0.95 ± 0.01
Avg Rel Improve & β	Rel Improve (%)			(β)	Rel Improve (%)		(β)
		2.43		0.92	3.33		0.94

Table 21: Complete accuracy results of ImageNet-pretrained ResNet-18 when transferred to 13 downstream datasets, steered with the Swish-only, SoftPlus-only, and combined (baseline) versions of CT (**bold** entries indicate improvement with CT). **While both the Swish-only and SoftPlus-only versions enhance model generalization, their improvements are less significant than the combined version, validating our CT implementation.** Reported values include means and standard deviations over three runs.

Dataset	CT Implementation	Swish only			SoftPlus only			Combination		
		ReLU (%)	+ CT (%)	(β)	ReLU (%)	+ CT (%)	(β)	ReLU (%)	+ CT (%)	(β)
Arabic Characters		86.49 ± 0.05	86.49 ± 0.05	1.00 ± 0.00	86.48 ± 0.12	89.90 ± 0.05	0.92 ± 0.00	86.46 ± 0.00	92.11 ± 0.08	0.70 ± 0.00
Arabic Digits		97.92 ± 0.03	97.99 ± 0.01	0.95 ± 0.01	97.91 ± 0.01	98.81 ± 0.02	0.89 ± 0.00	97.92 ± 0.03	98.92 ± 0.01	0.72 ± 0.04
Beans		85.94 ± 0.00	86.72 ± 0.00	0.92 ± 0.00	85.94 ± 0.00	94.53 ± 0.00	0.85 ± 0.00	85.94 ± 0.00	94.53 ± 0.00	0.60 ± 0.00
CelebA		87.88 ± 0.00	87.88 ± 0.00	1.00 ± 0.00	87.88 ± 0.00	88.53 ± 0.01	0.89 ± 0.01	87.88 ± 0.00	88.44 ± 0.00	0.75 ± 0.01
CUB-200-2011		62.93 ± 0.00	62.93 ± 0.00	1.00 ± 0.00	62.97 ± 0.04	64.13 ± 0.06	0.95 ± 0.00	62.93 ± 0.00	63.60 ± 0.00	0.90 ± 0.00
DTD		64.38 ± 0.03	64.38 ± 0.03	1.00 ± 0.00	64.41 ± 0.06	64.54 ± 0.03	0.95 ± 0.00	64.38 ± 0.03	64.50 ± 0.03	0.92 ± 0.00
Fashion MNIST		88.54 ± 0.02	88.54 ± 0.02	1.00 ± 0.00	88.53 ± 0.01	89.38 ± 0.02	0.94 ± 0.00	88.54 ± 0.02	89.52 ± 0.01	0.87 ± 0.01
FGVC-Aircraft		43.70 ± 0.11	43.82 ± 0.02	0.99 ± 0.01	43.74 ± 0.03	46.84 ± 0.06	0.91 ± 0.00	43.75 ± 0.06	48.30 ± 0.04	0.77 ± 0.01
Flowers102		87.80 ± 0.01	87.80 ± 0.01	1.00 ± 0.00	87.79 ± 0.01	88.59 ± 0.06	0.95 ± 0.00	87.80 ± 0.01	87.96 ± 0.01	0.86 ± 0.00
Food101		59.70 ± 0.05	59.74 ± 0.02	0.99 ± 0.01	59.77 ± 0.07	61.06 ± 0.05	0.93 ± 0.00	59.70 ± 0.05	60.48 ± 0.02	0.89 ± 0.02
MedMNIST (PathMNIST)		86.22 ± 0.01	86.27 ± 0.02	0.99 ± 0.00	86.23 ± 0.02	88.58 ± 0.10	0.90 ± 0.00	86.21 ± 0.00	87.27 ± 0.01	0.81 ± 0.00
MedMNIST (OCTMNIST)		65.47 ± 0.06	65.47 ± 0.06	1.00 ± 0.00	65.53 ± 0.15	67.27 ± 0.06	0.93 ± 0.00	65.47 ± 0.06	69.00 ± 0.26	0.80 ± 0.04
MedMNIST (DermaMNIST)		73.44 ± 0.03	74.03 ± 0.07	0.63 ± 0.01	73.39 ± 0.03	76.61 ± 0.00	0.88 ± 0.01	73.44 ± 0.03	77.74 ± 0.08	0.80 ± 0.01
Avg Rel Improve & β	Rel Improve (%)			(β)	Rel Improve (%)		(β)	Rel Improve (%)		(β)
		0.23		0.87	2.96		0.92	3.46		0.80

Table 22: Complete robust accuracy results of ImageNet-pretrained ResNet-18 under ℓ_2/ℓ_∞ adversarial attacks and common corruptions on CIFAR-10, CIFAR-100, and ImageNet, steered with the Swish-only, SoftPlus-only, and combined (baseline) versions of CT (**bold** entries indicate improvement with CT). **While both the Swish-only and SoftPlus-only versions enhance model robustness, their improvements are less significant than the combined version, validating our CT implementation.** Reported values include means and standard deviations over three runs.

(a) **Swish only.** Avg rel improve: 8.06%. Avg β : 0.99.

Attack \ Dataset	ℓ_2			ℓ_∞			Corruption		
	ReLU (%)	+ CT (%)	(β)	ReLU (%)	+ CT (%)	(β)	ReLU (%)	+ CT (%)	(β)
CIFAR-10	53.67 \pm 0.32	53.67 \pm 0.32	1.00 \pm 0.00	11.17 \pm 0.06	13.60 \pm 0.26	0.99 \pm 0.00	77.73 \pm 0.00	77.77 \pm 0.00	0.99 \pm 0.00
CIFAR-100	24.30 \pm 0.10	24.30 \pm 0.10	1.00 \pm 0.00	4.47 \pm 0.06	6.37 \pm 0.15	0.99 \pm 0.00	51.81 \pm 0.00	51.81 \pm 0.00	1.00 \pm 0.00
ImageNet	23.37 \pm 0.06	23.37 \pm 0.06	1.00 \pm 0.00	0.00 \pm 0.00	4.50 \pm 0.30	0.99 \pm 0.00	33.11 \pm 0.00	33.13 \pm 0.00	0.99 \pm 0.00

(b) **SoftPlus only.** Avg rel improve: 9.91%. Avg β : 0.98.

Attack \ Dataset	ℓ_2			ℓ_∞			Corruption		
	ReLU (%)	+ CT (%)	(β)	ReLU (%)	+ CT (%)	(β)	ReLU (%)	+ CT (%)	(β)
CIFAR-10	53.67 \pm 0.32	54.07 \pm 0.06	0.98 \pm 0.00	11.17 \pm 0.06	14.47 \pm 0.06	0.99 \pm 0.00	77.73 \pm 0.00	77.73 \pm 0.00	1.00 \pm 0.00
CIFAR-100	24.30 \pm 0.10	24.93 \pm 0.31	0.97 \pm 0.00	4.47 \pm 0.06	6.53 \pm 0.15	0.99 \pm 0.00	51.81 \pm 0.00	51.81 \pm 0.00	1.00 \pm 0.00
ImageNet	23.37 \pm 0.06	23.37 \pm 0.06	1.00 \pm 0.00	0.00 \pm 0.00	6.60 \pm 0.10	0.94 \pm 0.01	33.11 \pm 0.00	33.15 \pm 0.00	0.99 \pm 0.00